Pol. J. Environ. Stud. Vol. XX, No. X (XXXX), 1-22
DOI: *10.15244/pjoes/218207* ONLINE PUBLICATION DATE: 2026-03-18

Original Research

Multi-Scenario Analysis of Land-Use Change and Ecosystem Service Responses in Nyingchi Using the PLUS–InVEST–EOF Framework

Chengcheng Zou[1°], Wenbo Li[1, 2*], Zhen Xing[1], Jinxun Chen[1], Mingyu Dang[1], Wanqing Shen[1], Bingjie Bai[1]**

[1]Resources and Environment College, Xizang Agricultural and Animal Husbandry University, Nyingchi 860000, China
[2]Xizang Center for Human Settlement Research, Xizang Agricultural and Animal Husbandry University, Nyingchi 860000, China

Received: 25 July 2025
Accepted: 17 February 2026

Abstract

Spatiotemporal changes in land-use patterns reconfigure ecosystem service provision, making it critical to quantify these responses for planning in ecologically fragile plateau regions. Land-use in Nyingchi to 2030 was projected under multiple scenarios using the PLUS model; seven ES indicators and a composite ecosystem service (CES) index were quantified. Spatiotemporal modes and dominant drivers were assessed by combining Gi* hotspot and coldspot analysis with empirical orthogonal function (EOF) decomposition. Results: (1) Built-up land increased by 18.68 km² in 2000-2010 (dynamic degree 28.23%) and 28.96 km² in 2010-2020; by 2030, built-up land is projected to increase by an additional 30.49 km² under the urban development (UD) scenario relative to 2020. (2) From 2000 to 2020, water yield and soil retention declined by 29.7% and 49%; water purification weakened (higher nitrogen and phosphorus exports); carbon storage fluctuated narrowly; and habitat quality stabilized at 0.734 after 2010. In 2030, water yield and carbon storage are projected to fall under UD, whereas higher values across services are projected under the ecological protection scenario. (3) CES hotspots contracted southward and became more fragmented; in 2030, the UD scenario shows the largest increase in coldspot area (+5.90% relative to 2020). (4) The dominant spatiotemporal mode (EOF_1) paralleled rapid urbanization, and negative EOF_1-loading areas overlapped ecosystem service coldspots, suggesting potential path-dependent degradation in low-CES regions. Accordingly, we quantified county-level EOF_1 loadings and delineated three differentiated management units. These results provide quantified, comparable evidence for territorial spatial planning and ecological protection in Nyingchi, and a methodological reference for similar high-altitude regions.

Keywords: ecosystem services, EOF analysis, multi-scenario simulation, PLUS-InVEST model, Nyingchi

*e-mail: liwenbo@xza.edu.cn
**e-mail: xztibet-an@163.com
°ORCID iD: 0009-0009-2063-1356

Introduction

Ecosystem services (ESs) are the pathways through which ecosystem structure and function generate benefits for people. This relationship is formalized in the IPBES Global Assessment and tracked under the United Nations Sustainable Development Goals, particularly SDG 11 ("Sustainable Cities and Communities") and SDG 15 ("Life on Land") [1]. Rapid urban expansion has fragmented landscape structure and reduced provisioning, regulating, and cultural services in both established and emerging metropolitan regions, widening gaps between ESs supply and societal demand [2-4]. Among anthropogenic drivers, land use conversion is a direct and measurable control on the spatiotemporal dynamics of ESs bundles, shaping both their overall magnitude and spatial heterogeneity [5]. Quantifying how alternative land use trajectories reshape regional ES portfolios is therefore needed to evaluate development pathways against sustainability objectives.

In recent years, research on land use and ESs has advanced significantly, with growing scholarly focus on their conceptual frameworks, quantification methods, and spatiotemporal dynamics [6]. Within this field, methods for simulating land use change have matured and are generally categorized into 3 groups [7]: (1) Rule-driven cellular automata (CA) – including models such as CA-Markov [8, 9], OS-CA [10], EL-CA [11], CLUE-S [12], and SLEUTH [13]. These models simulate parcel dynamics on a grid using explicit transition rules and probabilities. They offer transparent rules and efficiently reproduce spatial patterns; however, they are limited in capturing cross-regional interactions, continuous succession across multiple land types, and responses to policy shocks. (2) Statistics- and machine learning-driven approaches – such as logistic regression [14] and ANN-CA [15]. These methods infer conversion probabilities from historical change and multidimensional drivers. While adaptable and capable of capturing nonlinear relationships, they are sensitive to data quality, less interpretable, and uncertain when extrapolated. (3) Hybrid scenario- and policy-constrained approaches – exemplified by FLUS [16] and PLUS [17]. These models combine pixel-level suitability and neighborhood competition with macro-level constraints (e.g., scenario-based policy quotas) to simulate land use evolution. They are useful for modeling human-land interactions and the co-evolution of multiple land types, and are well-suited to scenario analysis. Nevertheless, their outcomes depend on the plausibility of scenario assumptions and the accuracy of parameterization [18, 19]. In practical applications, these models are widely used tools for scenario-based ES assessment. For example, Jin et al. [20] coupled the PLUS model with quantitative assessments of multiple ESs to compare trade-offs and synergies across scenarios, providing comparable evidence for decision-making. Yang et al. [21] integrated multi-objective programming (MOP) with the PLUS framework to evaluate the potential of ecosystem carbon storage to contribute to regional emission reductions under future scenarios, demonstrating an integrated assessment pathway. Furthermore, Hwang et al. [13] used the SLEUTH model to project future land use scenarios and combined it with the InVEST model to assess changes in carbon storage. Their work revealed that protected areas can simultaneously exert development suppression and development substitution effects [22].

Regarding ESs assessment tools, mainstream approaches can be grouped into 3 types: the SolVES model, which emphasizes social preferences [23]; the ARIES platform, an integrated reasoning system based on semantic knowledge [24]; and the InVEST model, grounded in biophysical processes [25]. While all 3 support quantitative accounting, spatial representation, and scenario comparison of ESs, each has distinct emphases and limitations [26, 27]. SolVES maps the spatial distribution of public preferences and social values, but its cross-regional application is constrained by the availability and comparability of survey data [23]. ARIES automates inference of ESs supply, demand, and flow via knowledge-graph reasoning, yet generalized deployment depends on high-quality data and specialized platform support [28]. InVEST centers on the linkage between nature and human well-being; its open-source, modular architecture enables parallel assessment of multiple urban-relevant services (e.g., urban cooling, stormwater management, green-space accessibility) [29-31] and can quantify how much, where, and who benefits. Applications across regions indicate broad transferability [32]. Representative applications include [33], who developed a regionally customizable cloud-based model on ARIES to jointly characterize service supply, demand, and flow for cross-scenario comparison, and [34], who used InVEST to assess ESs supply under stakeholder-defined scenarios with sensitivity analysis to identify key drivers.

While previous research integrating land use modeling with ESs assessment has provided an important foundation, several challenges remain in developing a deeply coupled framework for land use-ESs trade-off analysis. These include: (1) Incomplete characterization of dynamic ESs interrelationships. Many studies lack a systematic analysis of how links among ESs change over time and across scenarios, limiting the identification of evolving synergies and trade-offs. (2) Geographical bias in study regions. Evidence is concentrated in developed plain areas, whereas strategic regions such as plateaus remain understudied. (3) Limited understanding of joint effects among multiple ESs. The combined effects of multiple ESs are insufficiently emphasized; comprehensive evaluation frameworks are still developing, and analyses of interactive mechanisms remain weak [35, 36].

Finally, in the assessment of composite ecosystem services (CES), technical frameworks – such as natural breaks classification and Gi* hotspot and coldspot analysis – can identify the spatial heterogeneity

and clustering of service bundles [37, 38]. However, most studies remain focused on static pattern description. Analyses of the intrinsic drivers that govern the spatiotemporal dynamics of CES are still limited, which reduces the value of current evidence for adaptive management and targeted policy design.

As the core area of the ecological security barrier at the southeastern edge of the Qinghai-Tibet Plateau, Nyingchi plays a prominent ecological role [39]. In recent years, intensified regional development has restructured land use patterns and affected the supply of ESs [40, 41]. Against this backdrop, we establish a PLUS-InVEST-EOF coupled framework for Nyingchi: PLUS simulates 2030 multi-scenario land use; InVEST quantifies key ESs; and EOF decomposition [42], combined with Gi* hotspot and coldspot analysis, identifies dominant spatiotemporal modes of the composite ESs (CES) index and their correspondence with land use change (Fig. 1). Within this framework, we address three objectives: (1) How do the scale and spatial trajectory of construction land expansion evolve across historical periods, and how are they projected to change under 2030 scenarios? (2) How did seven regulating services change during 2000-2020, and do they show differentiated responses across 2030 scenarios – particularly, is the urban-development scenario associated with the most adverse changes? (3) What are the spatiotemporal dynamics of ESs hotspots and coldspots in Nyingchi, and are these patterns linked to the dominant modes revealed by EOF? The answers to these questions, together with clarification of the underlying patterns, support the core objective of this study: to provide quantified, comparable evidence for formulating strategies on land-resource allocation and ecological conservation and restoration in Nyingchi, while offering methodological insights relevant to the management of fragile high-altitude ecosystems.

Materials and Methods

Study Region

Nyingchi is located in the southeastern part of the Xizang Autonomous Region (92°10'-98°50'E, 27°30'-30°50'N), within the middle and lower reaches of the Yarlung Tsangpo River basin, and covers approximately 114,000 km² (Fig. 2). The region features alpine and valley landscapes, pronounced topographic relief, and an average elevation of about 3,000 m. The climate comprises northern tropical margins, subtropical mountainous humid zones, and plateau temperate semi-humid zones, exhibiting distinct vertical zonation [40]. Precipitation mainly occurs in the summer, with mean

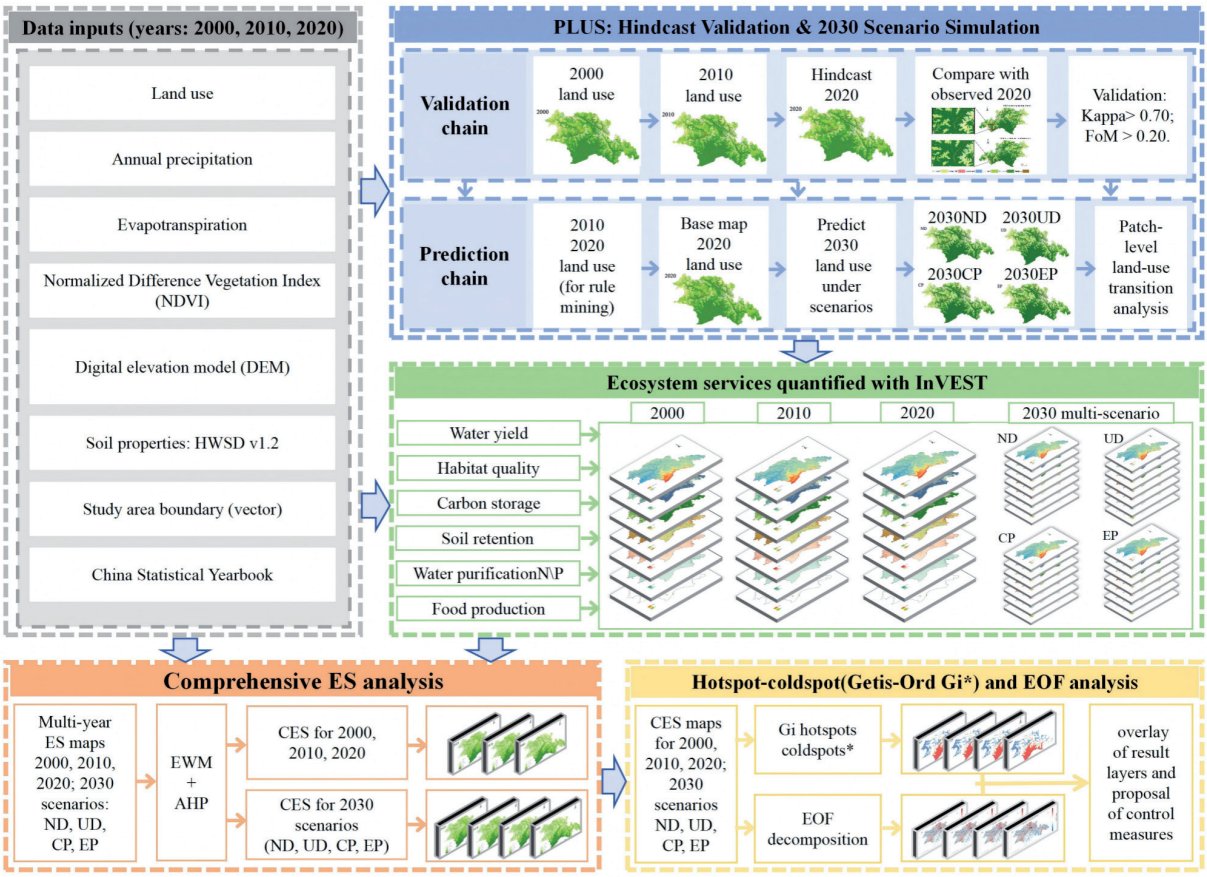

Fig. 1. Research framework.

annual rainfall of about 650 mm and a mean annual temperature of 8.7°C. Forest cover is 53.6%, making Nyingchi the third-largest forested region in China. This extensive forest endows the area with remarkable biodiversity and has earned Nyingchi the title of a "biological gene pool" [41]. Research on multi-scenario land use simulation and ESs responses in Nyingchi holds significant scientific value and provides important guidance for coordinating regional urban development with ecological protection.

Data Sources and Processing

The multi-source datasets used in this study are listed in Table 1. All datasets were preprocessed in ArcGIS Pro 3.1.2: raster data were uniformly resampled to 30 m, reprojected to the WGS 84 Mercator projection, and clipped to the study area boundary.

Research Methods

PLUS Model

The PLUS (Patch-generating Land Use Simulation) model is a cellular automaton-based framework that incorporates both natural and anthropogenic drivers to simulate land use change [43]. It comprises two core modules: LEAS (Land Use Expansion Analysis Strategy) and CARS (Multi-Type Random Patch Seeding), which together predict future land use distributions.

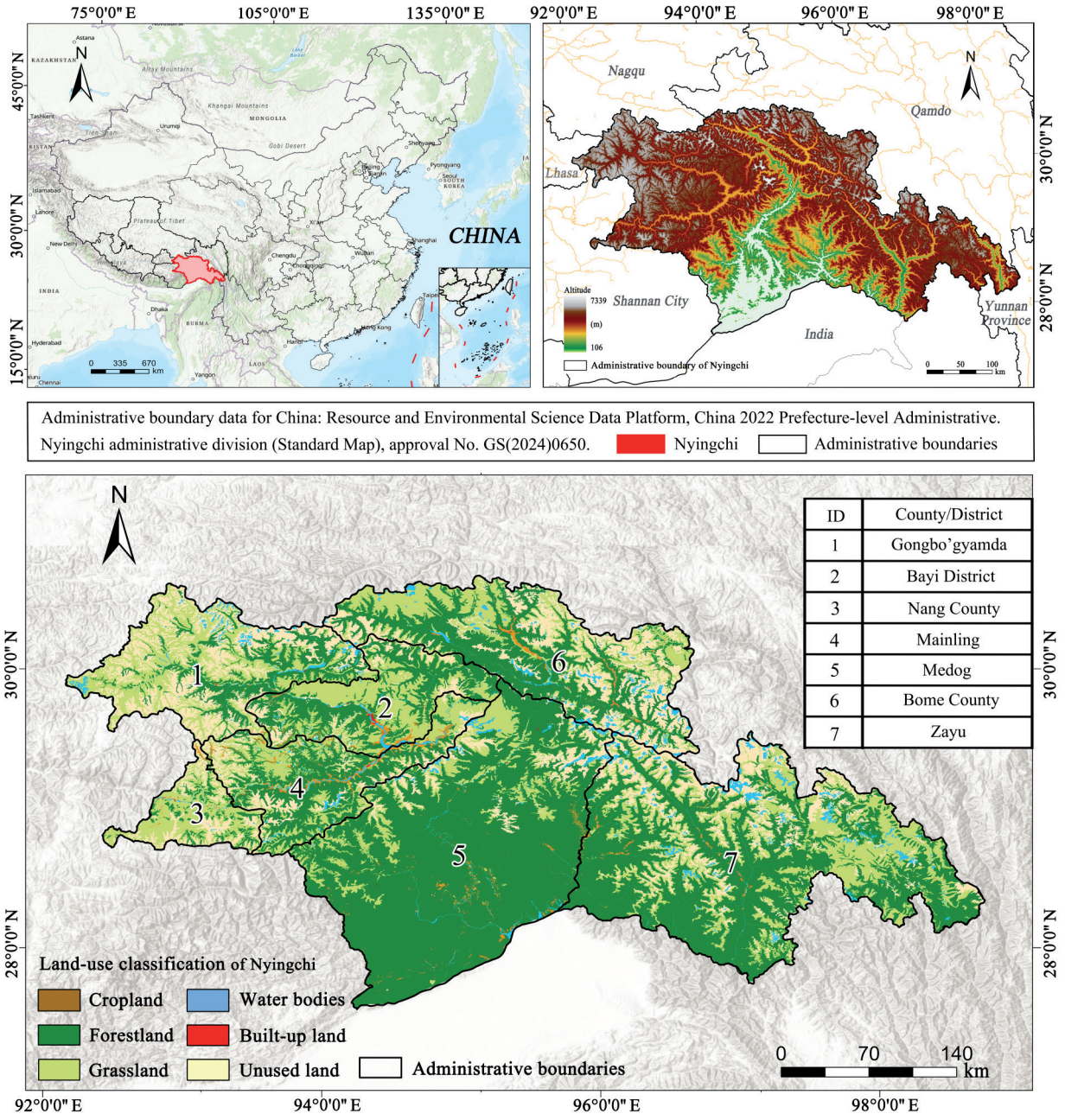

Fig. 2. Location and extent of Nyingchi, China.

Table 1. Data source and description.

Data name	Time period	Native resolution	Data type	Data source	Pre-processing	Accessed on
Land Use Data (CNLUCC)	2000, 2010, and 2020	30 m	TIFF	Resource and Environmental Science Data Platform (https://www.resdc.cn/)	Reclassified into six classes Reprojected to WGS 84 Mercator Clipped to the study area	2025-04-17
Annual Average Precipitation Data	2000, 2010, and 2020	1 km	TIFF	National Earth System Science Data Center (http://www.geodata.cn/)	Resampled to 30 m Reprojected to WGS 84 Mercator Clipped to the study area	2025-04-23
Evapotranspiration Data	2000, 2010, and 2020	1 km	TIFF	National Earth System Science Data Center (http://www.geodata.cn/)	Resampled to 30 m Reprojected to WGS 84 Mercator Clipped to the study area	2025-04-23
Based on the World Soil Database v1.2 (HWSD)	Static	1 km	TIFF	National Cryosphere Desert Data Center (http://www.ncdc.ac.cn/)	Extraction of four soil properties-Clay (Mc), Silt (Msilt), Sand (Ms), and Organic carbon (orgC). Resampled to 30 m Reprojected to WGS 84 Mercator Clipped to the study area	2025-04-17
Elevation Data (DEM)	Static	30 m	TIFF	Japan Aerospace Exploration Agency (https://www.eorc.jaxa.jp/ALOS/)	Sink filling ×2 Reprojected to WGS 84 Mercator Clipped to the study area	2025-04-17
Normalized Difference Vegetation Index (NDVI)	2000, 2010, and 2020	30 m	TIFF	National Science Technology Infrastructure (http://www.nesdc.org.cn/)	Reprojected to WGS 84 Mercator Clipped to the study area	2025-04-17
Research Area Vector Boundary (GS20240650)	Static	/	SHP	Standard Map Service of the Ministry of Natural Resources of China (http://bzdt.ch.mnr.gov.cn/)	Clip to the administrative boundary of the study area	2025-04-17
China Statistical Yearbook	2000, 2010, and 2020	/	TABLE	National Bureau of Statistics (http://www.stats.gov.cn/)	Filtered multi-period grain production for Nyingchi (10^4 t)	2025-04-28
Hydrological data	2000, 2010, and 2020	/	SHP	HydroSHEDS 2024 dataset (https://www.hydrosheds.org/)	Clip to the administrative boundary of the study area	2025-04-23
China Multi-Period Road Spatial Distribution Data	2000, 2010, and 2020	/	SHP	Resource and Environmental Science Data Platform (https://www.resdc.cn/)	Clip to the administrative boundary of the study area	2025-04-17
China GDP Spatial Distribution 1-km Grid Dataset	2000, 2010, and 2020	1 km	TIFF	Resource and Environmental Science Data Platform (https://www.resdc.cn/)	Resampled to 30 m Reprojected to WGS 84 Mercator Clipped to the study area	2025-04-17
China Population Spatial Distribution 1-km Grid Dataset	2000, 2010, and 2020	1 km	TIFF	Resource and Environmental Science Data Platform (https://www.resdc.cn/)	Resampled to 30 m Reprojected to WGS 84 Mercator Clipped to the study area	2025-04-17

Note: The multi-period land use primary classes and their corresponding secondary classes are as follows: Cropland (paddy field, dryland cropland); Forestland (closed forest, shrubland, open forest, other forestland); Grassland (high-coverage grassland, medium-coverage grassland, low-coverage grassland); Water bodies (rivers and channels, lakes, reservoirs and ponds, permanent ice and snow, tidal flats, river and lake beaches); Urban–rural, industrial–mining, and residential land (urban land, rural residential areas, other construction land); Unused land (sandy land, Gobi, saline–alkali land, marshland, bare land, bare rocky land, other).

(1) The LEAS module applies rules for expansion, contraction, and conversion, combined with random forest algorithms, to classify land use expansion samples based on driving factors and to calculate the development probability P_i for each land use type [44]:

$$P_{i,k}^{d}(x) = \frac{\sum_{n=1}^{M} I(h_n(x) = d)}{M} \quad (1)$$

where x is a vector of multiple driving factors; I is an indicator function for the set of decision trees; $h_n(x)$ denotes the prediction result of the n-th decision tree for vector x; and M is the total number of decision trees.

In the LEAS module, the random forest was configured with 20 regression trees (M = 20), with a sampling rate of 0.01 and mTry = 3.

(2) The CARS module is based on stochastic seed generation and threshold-decreasing rules to model patch growth and conversion processes [45]. The transition probability is defined as follows:

$$OP_{i,k}^{d=1,t} = P_{i,k}^{d=1} \times \Omega_{i,k}^{t} \times D_{k}^{t} \quad (2)$$

where $OP_{i,\ k}^{d=1,t}$ denotes the probability that the i-th patch transforms to land class k at time t; Ω_k^t denotes the domain effect of pixel i; and $D^t_{i,k}$ represents the future effect on land class k.

In the CARS module, the neighborhood size was set to 3 (3×3), with a patch generation threshold of 0.1, an expansion coefficient of 0.01, and a seed percentage of 0.01 (Thread = 1).

Multi-scenario Simulation and Model Validation

Four scenarios were developed to explore alternative development pathways – natural development (ND), urban development (UD), cropland protection (CP), and ecological protection (EP). Scenario parameters were determined from previous studies [14, 46] and from the territorial spatial planning documents for Nyingchi's seven counties (2021-2035; People's Government of the Xizang Autonomous Region, Government Letters [2024] No. 45 and No. 54) [47, 48] (Table 2). Table 2 summarizes narrative scenario settings (probability adjustments); the full binary 0/1 transition matrices are provided in Supplementary Table S1.

The 2020 land use simulation was evaluated using the Kappa and FoM coefficients (both ranging from 0 to 1). A Kappa>0.70 is generally interpreted as high agreement, and a FoM>0.20 is often taken to indicate a usable simulation, with larger values implying greater reliability [17, 49].

Given the critical role of built-up land expansion in scenario simulations, we conducted a one-at-a-time (OAT) sensitivity test on the built-up land neighborhood weight in the PLUS model. Using 2020 as the baseline year, while keeping the expansion probability surface generated by the LEAS module unchanged, we perturbed the neighborhood weight for built-up land by ±10% and ±20% relative to its initial setting and compared the simulation accuracy under different parameter values. The results show that within this perturbation range, fluctuations in overall accuracy, Kappa, and FoM were negligible (standard deviation < 0.1), and the spatial pattern of built-up land expansion remained highly consistent based on visual comparison. These findings indicate that the PLUS model developed in this study is stable with respect to single-parameter perturbations and is suitable for subsequent multi-scenario simulations.

Model Parameterization

We use a binary land use conversion matrix in which 0 prohibits conversion from a source to a target class, and 1 permits it. The matrix is constructed by synthesizing prior studies on land use convertibility [50] and by aligning with China's "Three Zones and Three Lines" spatial regulation system and the rules for

Table 2. Scenario settings and conversion rules.

Scenario type	Conversion rules
Natural development (ND)	This scenario is based on land use evolution patterns from 2010 to 2020 and excludes policy interventions. The Markov Chain module within the PLUS model was used to project land use demand for 2030 under natural development conditions [14, 46]
Urban development (UD)	This scenario focuses on infrastructure development and the enhancement of service capacity. The conversion probabilities from cropland, forestland, and grassland to built-up land were increased by 20%. Meanwhile, the conversion probabilities from built-up land to other land types (except cropland) were reduced by 30% [14, 46]
Cropland protection (CP)	This scenario is aligned with the "four zones" functional zoning outlined in Xizang Government Letter [2024] No. 54, and prioritizes cropland resource protection and food security. Expansion of built-up land was restricted, and the conversion probability from cropland to built-up land was reduced by 60% [47, 48]
Ecological protection (EP)	This scenario follows the "dual ecological barriers" framework and aims to maximize ecological benefits through strict control of development activities. The conversion probabilities from forestland and grassland to built-up land were reduced by 50%, and the probability of cropland being converted to built-up land was reduced by 30% [47, 48]

permanent basic farmland [51]. Ecological redlines and permanent basic farmland act as rigid bottom lines: cells falling within these zones are non-convertible to built-up across all scenarios [47, 52]. Nyingchi's statutory urban construction boundary constrains urban growth; any permitted outward expansion is limited to contiguous extensions of existing built-up areas and corridors along major transport routes, and must remain outside strictly protected areas and permanent basic farmland. Scenario settings follow local planning guidance and documented urbanization patterns: in the baseline, small, quota-controlled expansions outside the boundary are allowed under the above safeguards; in UD, the probability of such outward extensions is moderately elevated while all safeguards remain in force; in CP and EP, conversion to construction land is most restrictive, fully enforcing the hard constraints. The full, scenario-specific transition matrices are provided in Supplementary Table S1, and the preparation of constraint rasters (data sources, preprocessing, and masking order) is detailed in Supplementary Methods.

Neighborhood weights characterize each land use class's expansion potential within its neighborhood; their values range from 0 to 1, with higher values indicating greater propensity to expand. Drawing on the study area's historical land use evolution, following [53], and through iterative calibration and validation in the PLUS model, we ultimately determined neighborhood-weight parameters that yield high simulation accuracy (Supplementary Table S2).

Ecosystem Services Evaluation

InVEST Model

To enhance the accuracy of ESs evaluation while considering both natural and anthropogenic characteristics of Nyingchi, seven ES indicators were selected: water yield, habitat quality, carbon storage, soil retention, water purification (nitrogen and phosphorus), and food production. The InVEST model was used to assess each ES indicator (Table 3) quantitatively. The key parameters for each ES module in this study are specified with reference to prior work and relevant Xizang-specific local datasets [54-56]. For the InVEST Water Yield module, the Budyko seasonality factor was set to Z = 15. Full parameter tables are provided in the Supplementary Information (Supplementary Tables S3-S9).

To evaluate how uncertainty in key InVEST parameters influences simulation outcomes, we conducted a one-at-a-time (OAT) sensitivity analysis for the major ecosystem service modules. For the Water Yield module, plant available water content (PAWC) and the seasonality constant (Z) were selected as the primary uncertain parameters, and were perturbed by ±10% and ±20% around the baseline scenario. The results indicate that the relative changes in simulated water yield were all < 3%, and the spatial pattern remained stable, suggesting that parameter uncertainty does not materially affect the main conclusions of this module.

Table 3. Selection of ES indicators and calculation formulas.

Ecosystem services	Calculation formula	Formula interpretation
Water yield	$Y_{xj} = \left(1 - \frac{AET_x}{P_x}\right) \times P_x$	Y_{xj}: Annual water yield for land use type j in pixel x (mm) AET_x: Annual evapotranspiration for land use type j in pixel x (mm) P_x: Annual precipitation in pixel x (mm)
Habitat quality	$Q_{xj} = H_j \left[1 - \frac{{D^z}_{xj}}{{D^z}_{xj} + k^z}\right]$	Q_{xj}: Habitat quality for land use type j in pixel x D_{xj}: Threat level K: Half-saturation constant H_j: Habitat suitability for land use type j Z: Normalization constant
Carbon storage	$CS = C_{above} + C_{below} + C_{dead} + C_{soil}$	C_{above}: Aboveground vegetation carbon content (t/ha) C_{below}: Belowground vegetation carbon content (t/ha) C_{dead}: Carbon content in dead organic matter (t/ha) C_{soil}: Soil carbon content (t/ha)
Soil retention	$USLE_i = R_i \times K_i \times LS_i \times C_i \times P_i$	R_i: Rainfall erosivity factor (MJ·mm·ha^{-1}·h^{-1}) K_i: Soil erodibility factor (t·h·MJ^{-1}·mm^{-1}) LS_i: Slope length-gradient factor (dimensionless) C_i: Vegetation cover factor (dimensionless) P_i: Support practice factor (dimensionless)
Water purification	$NDR_i = NDR_{0,i} \times \left[1 + exp\left(\frac{IC_0 - IC_i}{k}\right)\right]^{-1}$	$NDR_{0,i}$: Proportion of nutrients not retained by downslope pixels IC_i: Topographic index IC_0: Calibration parameter k: Calibration parameter
Food production	$Y_{mod\_GC} = min\{Y_N, Y_P, Y_K\}$	Y_{mod_GC}: Potential yield for cropland pixel x (t·ha^{-1}) Y_N: Yield under nitrogen limitation (t·ha^{-1}) Y_p: Yield under phosphorus limitation (t·ha^{-1}) Y_K: Yield under potassium limitation (t·ha^{-1})

For the Carbon Storage module, carbon density values for cropland, forestland, and built-up land were adjusted by ±20%; the total carbon stock varied by <5%, with an essentially consistent spatial pattern, indicating low sensitivity to carbon density inputs and robust outcomes. For the Habitat Quality module, we sequentially modified the weight, maximum effective distance, and decay function type of each threat factor using an item-by-item adjustment approach. The results show moderate sensitivity in localized areas – particularly to changes in maximum effective distance and threat weights – whereas the overall spatial distribution exhibited only minor changes, demonstrating good robustness of the module under parameter perturbations.

Comprehensive Ecosystem Service Assessment System Construction (CES)

The entropy weight method (EWM) objectively determines the importance of indicators by measuring parameter deviation, thereby effectively minimizing the randomness associated with subjective weighting assignments [57]. However, ESs exhibit pronounced spatial heterogeneity across regions, making single-objective or single-subjective weighting approaches susceptible to distribution bias. To address this issue, a weighted integration approach combining entropy weighting and the analytic hierarchy process (AHP), each contributing equally (50%), was applied to construct the CES assessment system [58, 59]. This method enhances the scientific rigor and objectivity of ES quantification in Nyingchi [7]. The calculation is defined as follows:

$$CES = \sum_{i=1}^{n} \omega i \cdot S_{i,t} \tag{3}$$

$S_{i,t}$ is the normalized value of the i-th ecosystem service in year t; n is the number of ES indicators. Through the integrated application of EWM and AHP, the respective weights for water yield, habitat quality, carbon storage, soil retention, water purification (nitrogen and phosphorus), and food production were determined as 0.2097, 0.2066, 0.1136, 0.2167, 0.0950, 0.0934, and 0.0650, respectively.

*Hotspot and Coldspot Analysis Based on the Getis-Ord Gi**

Hotspot and coldspot analysis is a GIS-based spatial statistical method that visually reveals the spatial distribution of high-value (hotspot) and low-value (coldspot) ES areas within the study region [60]. The Getis-Ord Gi* was employed to identify localized clusters of high and low values by calculating z-scores, where higher z-scores indicate hotspots and lower z-scores indicate coldspots [61, 62]. Analyses were run in ArcGIS Pro 3.1.2 with a Fixed Distance Band of 2,000 m and FDR-adjusted p-values.

Empirical Orthogonal Function (EOF) Analysis and North's Test

Empirical Orthogonal Function (EOF) analysis was used to extract dominant spatiotemporal patterns of CES. We decomposed the CES field $W(x, y, t)$ as:

$$W(x,y,t) = \sum_{i=1}^{K} \mathrm{C_n V_n(x,y)\, T_n(t)} \tag{4}$$

where $V_n(x,y)$ is the n-th spatial loading pattern and $T_n(t)$ is the associated temporal coefficient; K is the number of retained modes. Positive (negative) loadings indicate areas where CES tends to increase (decrease) as T_n increases. V_n and T_n are scaled to satisfy orthonormality constraints.

To assess mode separability, we applied North's empirical criterion. The sampling error of the i-th eigenvalue λ_i was estimated as:

$$\delta\lambda_i = \lambda_i \sqrt{\frac{2}{N_{edof}}} \tag{5}$$

with N_{edof} denoting the effective number of independent temporal samples. Two adjacent modes are considered statistically distinct when their error bands $\lambda_i \pm \delta\lambda_i$ do not overlap.

Results

Land Use Change and Multi-Scenario Simulation Analysis

Land Use Change Analysis from 2000 to 2020

Land use data for Nyingchi from 2000 to 2020 (Fig. 3) were quantified by area and used for comparative analysis (Table 4).

From 2000 to 2010, built-up land increased, with a dynamic degree of 28.23% and a net gain of 18.68 km². Water bodies recorded the largest contraction, with a dynamic degree of -6.09% and a loss of 5,046.91 km². During this decade, cropland and forestland increased slightly, whereas water bodies and unused land decreased markedly, indicating a pronounced shift in land use structure. From 2010 to 2020, built-up land continued to expand, although more slowly, with a dynamic degree of 11.55% and a net gain of 28.96 km². Cropland declined slightly, with a dynamic degree of -0.19%, while other categories remained relatively stable. Overall, forestland and grassland remained the dominant types and showed only minor area fluctuations, maintaining a comparatively stable land use pattern.

Chord diagram analysis for 2000-2010 (Fig. 4a)) indicates that water bodies and unused land were

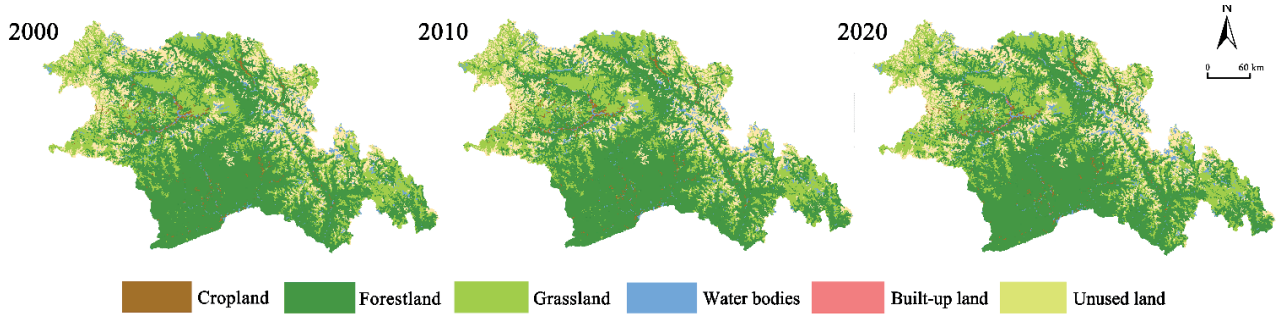

Fig. 3. Land use classification for 2000, 2010, and 2020.

Table 4. Analysis of land use dynamics and area changes, 2000, 2010, and 2020.

Typology	2000-2010 Dynamic degree (%)	2010-2020 Dynamic degree (%)	2000-2010 Area change (km^2)	2010-2020 Area change (km^2)
Cropland	9.13%	-0.19%	601.85	-24.19
Forestland	0.38%	-0.01%	2254.92	-26.43
Grassland	7.79%	-0.01%	13099.78	-0.21
Water bodies	-6.09%	0.05%	-5046.91	17.77
Built-up land	28.23%	11.55%	18.68	28.96
Unused land	-3.63%	0.01%	-10676.60	3.22

primarily converted to grassland, contributing 6,823.75 km² and 17,401.57 km², which correspond to 15.32% and 39.07% of the inflow to grassland, respectively. Grassland recorded a net gain of 21,703.21 km², with 46.36% originating from unused land. Cropland increased by 1,097.90 km², with 49.85% resulting from conversions out of grassland. Forestland increased by 13,221.22 km², with 47.70% originating from unused land. Built-up land increased by 21.83 km², with 49.26% of its inflow originating from grassland. The large declines in water bodies and unused land coincided with rapid economic development and increased anthropogenic disturbance, indicating that land-type conversion was most intense during this period.

From 2010 to 2020 (Fig. 4b)), built-up land expanded mainly at the expense of cropland, which accounted for 48.48% of the inflow to built-up land, while transfers among the other land categories were comparatively limited. This pattern indicates a more stable land use structure in the latter decade.

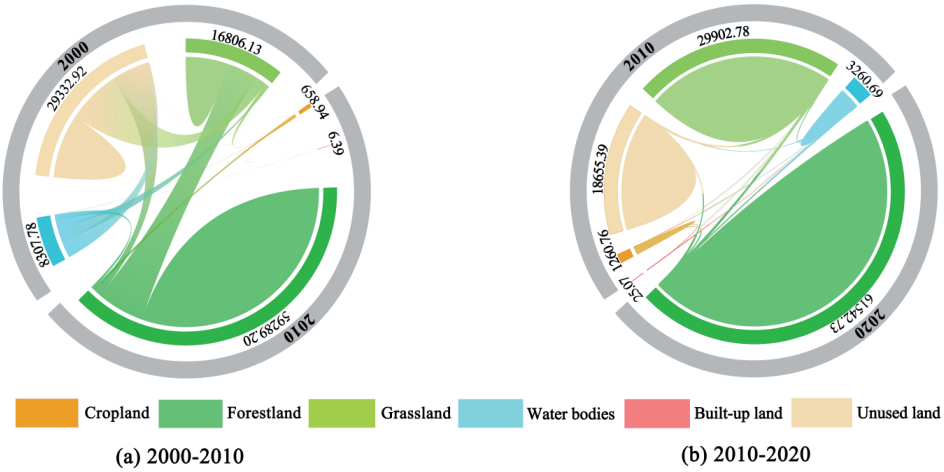

Fig. 4. Land use transfer matrix chord charts for 2000, 2010, and 2020.

PLUS Model Validation

To evaluate the simulation accuracy of the PLUS model, we simulated Nyingchi's 2020 land use pattern and compared the outputs with the observed map (Fig. 5). The simulation achieved an overall accuracy of 0.943, a Kappa coefficient of 0.905, and a FoM of 0.232, indicating high accuracy. The simulated spatial pattern closely matches the 2020 observations, supporting the model's suitability as a reliable basis for 2030 multi-scenario land use projections and quantitative ecosystem service analyses.

Multi-Scenario Land Use Simulation for 2030

Taking Nyingchi's natural and socio-economic conditions into account, we selected the following driving factors for simulation: elevation, slope, aspect, NDVI, annual precipitation, mean annual temperature, annual evaporation, distance to water bodies, distance to urban centers, distance to rural settlements, distance to the railway, distance to provincial roads, distance to county roads, GDP, and population (Fig. 6(a-o)). The PLUS model was then used to simulate land use patterns for 2030 under four scenarios: ND, UD, CP, and EP (Fig. 7).

Area changes and dynamic degrees for each land use type from 2020 to 2030 are reported in Table 5. Under the ND, water bodies and built-up land increased slightly by 17.17 km² and 23.73 km², respectively, while the other land use types contracted marginally; the dynamic degree of built-up land was 0.04%, and overall land use change remained moderate. Under the UD, built-up land increased by 30.49 km², with a dynamic degree of 0.06%, accompanied by the largest reductions in forestland, cropland, and grassland among the four scenarios, whereas changes in water bodies were minimal. Under the CP, cropland rebounded slightly, increasing by 2.11 km², and built-up land expanded by 14.39 km² with a dynamic degree of 0.03%; other land use types showed negligible changes. Under the EP, forestland contracted the least, decreasing by 31.07 km², grassland increased by 3.83 km², and built-up land exhibited the smallest expansion at 12.30 km², with a dynamic degree of 0.02%, thereby maintaining a relatively stable overall land use structure. Across all four scenarios, water bodies and built-up land generally expand, whereas forestland and unused land tend to contract. Built-up land shows a persistent positive dynamic degree across scenarios, suggesting a continued expansion signal under the stated assumptions.

ES Multi-Scenario Spatiotemporal Evolution Analysis

Spatiotemporal variations in ESs from 2000 to 2030 in Nyingchi are evident (Fig. 8). Water yield declined from 564.579 mm in 2000 to 397.136 mm in 2020 and is simulated to decrease by a further 4 mm across all four scenarios by 2030. Soil retention decreased from 15.226 t to 7.475 t over the same period, averaging about 7.18 t across the 2030 scenarios, with the ND showing the greatest decline. Habitat quality remained high, reaching 0.734 in 2010 and then stabilizing, with the EP showing the smallest decline. Carbon storage fluctuated slightly within the range 11.036 to 11.207 t throughout the study period. Water purification efficiency deteriorated, reflected by nitrogen export increasing from 0.0519 kg in

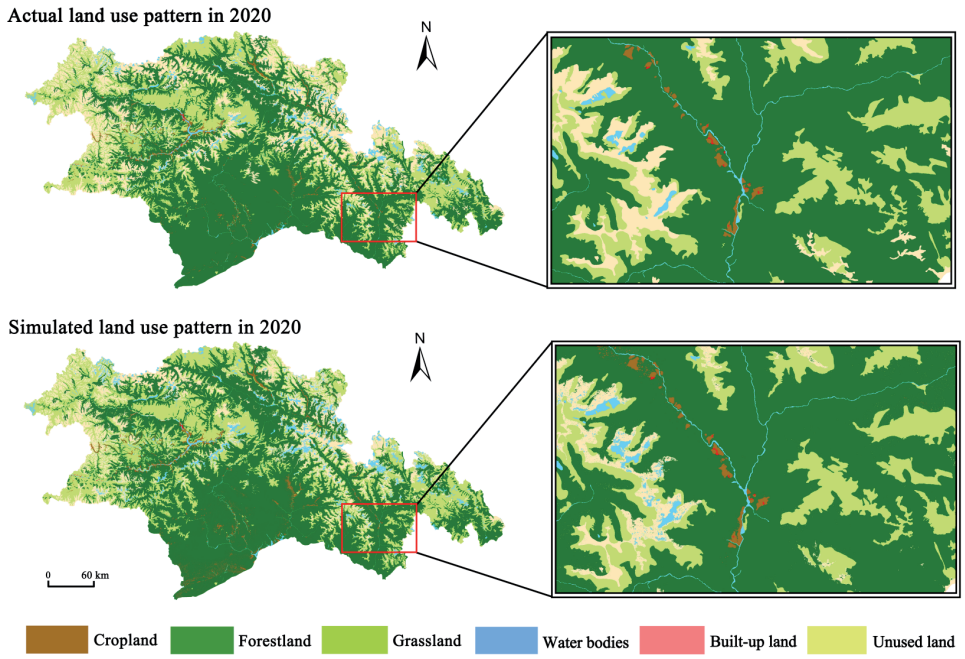

Fig. 5. Comparative analysis of actual land use classification and simulation results for 2020.

2000 to 0.0663 kg in 2020 and continuing to rise toward 2030, while phosphorus export increased moderately before stabilizing. Food production rose steadily from 0.127 kg in 2000 to 0.148 kg in 2020 and peaked at 0.164 kg under the CP in 2030.

Overall, water yield and soil retention declined, water purification efficiency worsened as nitrogen and phosphorus export increased, habitat quality and carbon storage remained broadly stable, and food production continued to improve.

Spatial patterns of ESs under the four 2030 scenarios differ across the region (Fig. 9). Water yield decreases in all scenarios, with the ND showing the largest reduction and the EP the smallest, while high-value zones remain concentrated in Medog and Zayu counties. Habitat quality exhibits an expansion of low-value areas along

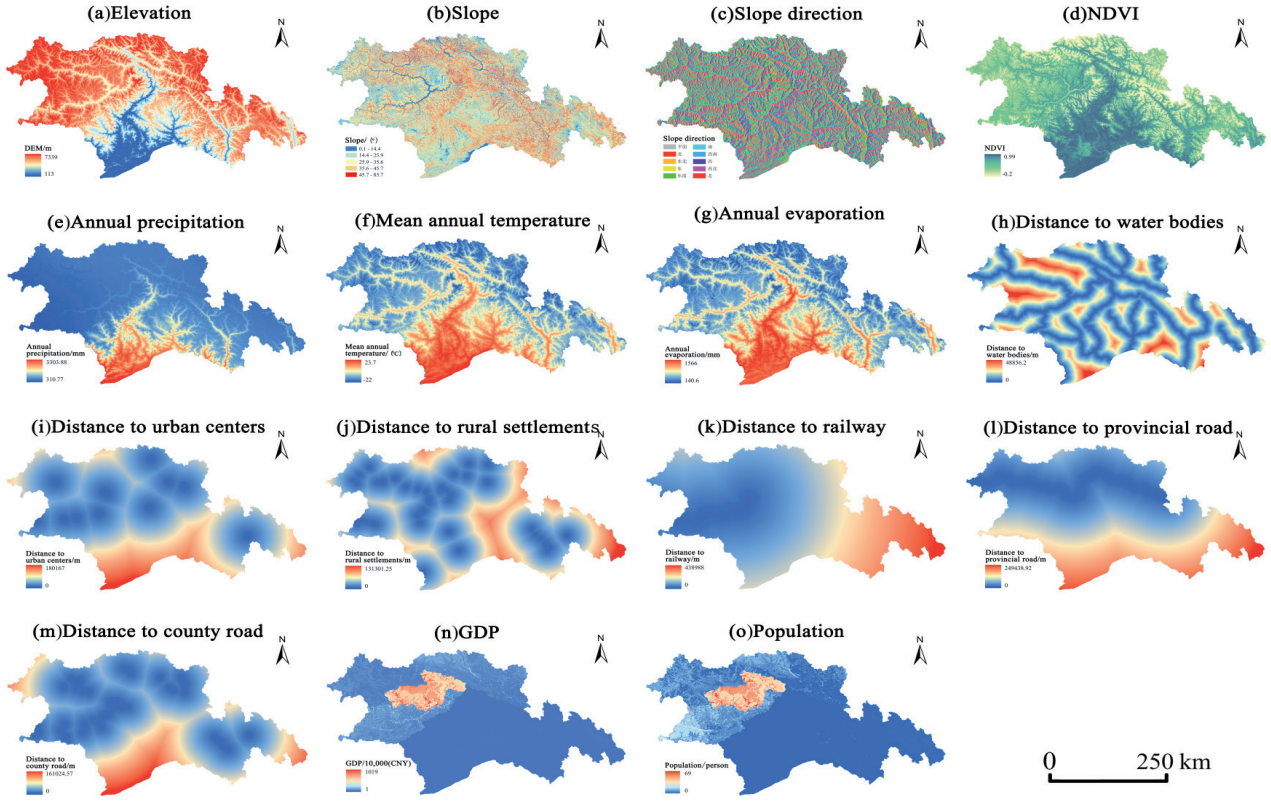

Fig. 6. Drivers of land use change.

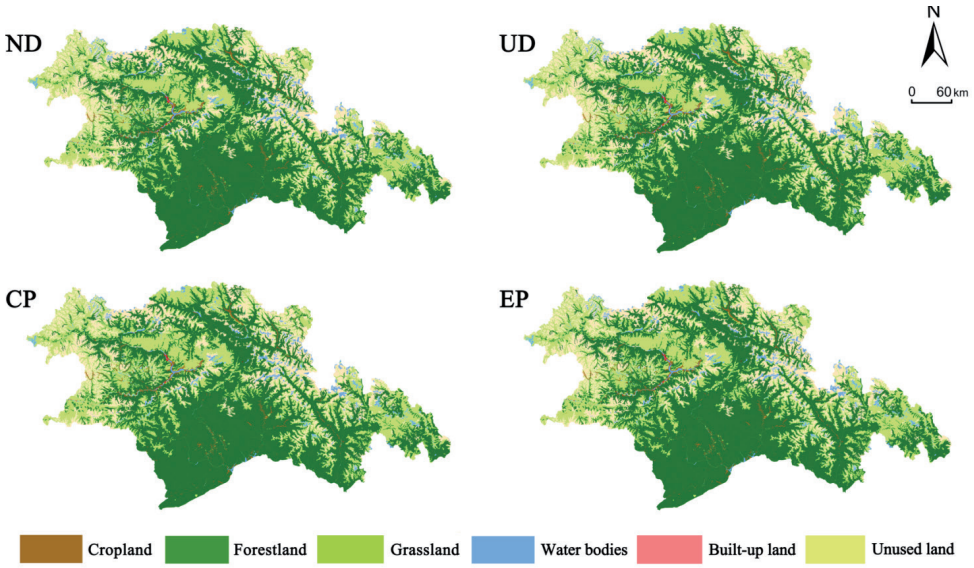

Fig. 7. Land use simulation results under multiple scenarios for 2030.

Table 5. Land use area and its changes under multiple scenarios in 2030.

Typology	Area of each scenario land use type in 2030				Changes in land use area and dynamics by scenario, 2020-2030							
					ND		UD		CP		EP	
	ND/km^2	UD/km^2	CP/km^2	EP/km^2	Area/km^2	Dynamic/%	Area/km^2	Dynamic/%	Area/km^2	Dynamic/%	Area/km^2	Dynamic/%
Cropland	1229.81	1226.93	1238.74	1234.29	-6.82	-0.01	-9.70	-0.01	2.11	0.01	-2.34	0.01
Forestland	61486.14	61484.86	61486.38	61488.77	-33.7	0.01	-34.98	0.01	-33.46	0.01	-31.07	0.01
Grassland	29906.38	29904.35	29906.44	29910.62	-0.41	0.01	-2.44	0.01	-0.35	0.01	3.83	0.01
Water bodies	3297.11	3296.55	3297.22	3297.16	17.17	0.01	16.61	0.01	17.28	0.01	17.22	0.01
Built-up land	77.77	84.53	68.42	66.34	23.73	0.04	30.49	0.06	14.39	0.03	12.30	0.02
Unused land	18664.35	18664.34	18664.36	18664.39	-0.13	0.01	-0.14	0.01	-0.12	0.01	-0.09	0.01

river valleys and transportation corridors under the ND and UD, whereas high-value areas remain largely contiguous under the CP and EP. Carbon storage shows an expansion of low-value zones in Bayi District under the UD; high-value forest areas in the northern and southern parts remain stable or slightly higher under the CP and EP. Soil retention shows a general decline, with the greatest losses under the ND, although the EP maintains relatively higher values in localized terrace regions. Water purification patterns remain broadly consistent with historical conditions, with minor fluctuations within ±3%. High-value areas for food production continue to concentrate in river-valley terraces, with the greatest enhancement under the CP and reduced spatial coverage under the UD, while food production capacity remains constrained by cropland extent and topographic conditions, leaving limited room for further increases.

From an integrated perspective of multiple ecosystem service indicators, the 7 services in the study area exhibit a clear structure of synergies and trade-offs. First, water yield and soil retention show a pronounced co-declining (synergistic) trend: both decreased synchronously from 2000 to 2020 and remain at relatively low levels across all 2030 scenarios. Spatially, their high-value areas are generally concentrated in humid mountain-valley transition zones with high forest cover, indicating that hydrological regulation and erosion control are jointly constrained by similar topographic and vegetation conditions. In contrast, water purification (represented by nitrogen export and phosphorus export) displays a typical trade-off with these regulating services: nitrogen export continues to increase over time and still rises toward 2030, whereas phosphorus export increases in earlier periods and then tends to stabilize, collectively implying increasing purification pressure. Meanwhile, the spatial distribution of water purification under the 2030 scenarios remains broadly consistent with historical patterns and shows only minor fluctuations, suggesting that the observed change mainly reflects a slight deterioration in overall levels rather than a fundamental reorganization of spatial patterns. Second, habitat quality and carbon storage remain generally high with limited fluctuations, reflecting a stable synergy; their spatial patterns closely track forest distribution, highlighting the key role of forest ecosystems in jointly supporting habitat functions and carbon sequestration. However, scenario contrasts also reveal localized vulnerability of this synergy: under scenarios with stronger urban expansion, low habitat-quality areas expand along river valleys and transportation corridors, and low carbon-storage zones enlarge around the Bayi District, whereas under cropland protection and ecological protection scenarios, high habitat-quality and high carbon-storage areas remain more contiguous and stable. Third, food production continues to increase and is strongly associated with the spatial concentration of cropland on river-valley terraces, with the largest gains under the cropland-priority scenario; however,

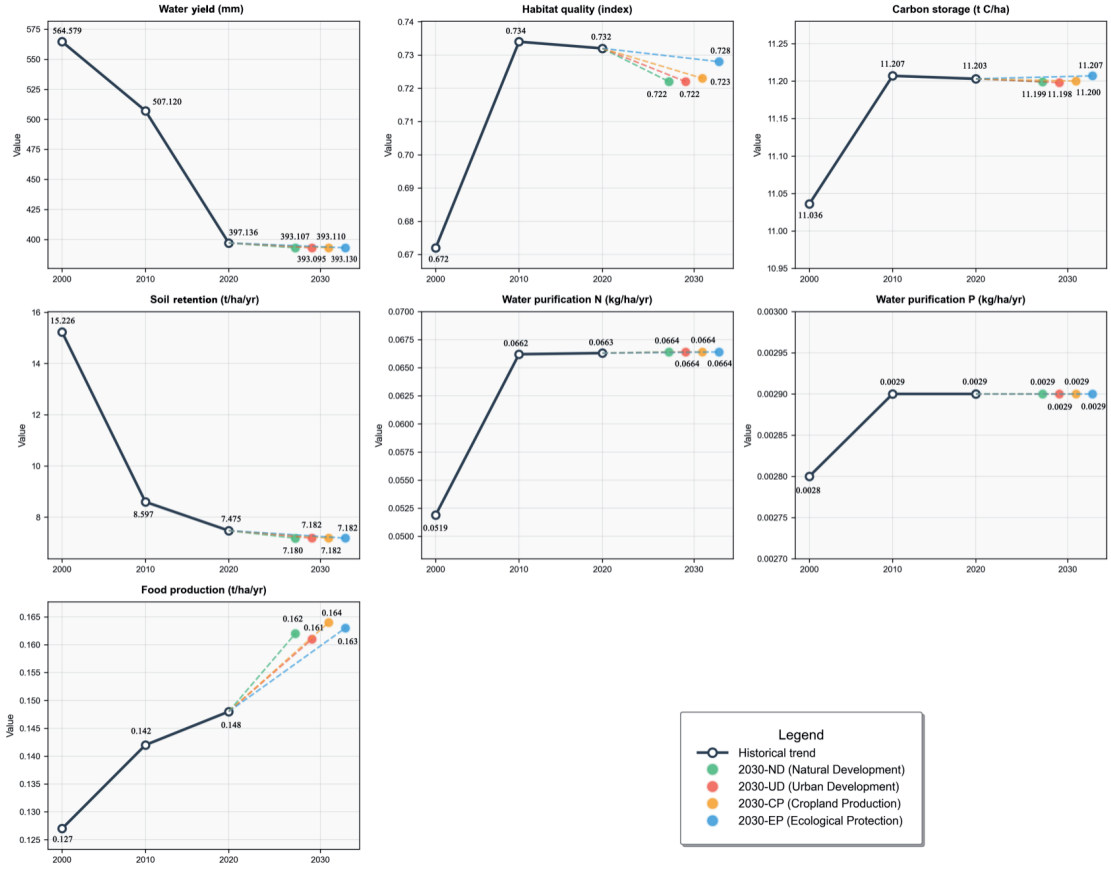

Fig. 8. Mean values of each ES under multiple scenarios for the base year and 2030.

these hotspots are largely located in valley zones with more intensive human activities, which are also more sensitive to habitat fragmentation and nutrient export, thereby highlighting a potential trade-off between enhanced provisioning services and increasing habitat and water-quality pressures. By comparison, the ecological-protection-oriented scenario more effectively constrains habitat-quality decline and maintains relatively higher soil retention in some areas, implying that limiting disorderly expansion in valley-corridor zones, maintaining connectivity among key ecological patches, and improving hillslope vegetation cover may help to alleviate conflicts between provisioning services and regulating/supporting services. Overall, the ecosystem service relationships in the study area can be summarized into two typical bundles: (i) a mountain-forest-dominated synergy bundle centered on carbon storage-habitat quality, which is highly consistent with the high-value patterns of regulating services such as water yield and soil retention; and (ii) a valley-dominated trade-off bundle driven by cropland use and built-up land expansion, in which increased food production is often accompanied by higher nutrient export risk and elevated habitat degradation pressure along valley corridors. This results in a spatial differentiation pattern characterized by relatively stable ecological functions in contiguous mountain areas and more concentrated trade-offs in river-valley zones.

CES Spatial Pattern and Evolution Analysis

CES Assessment System Construction

CES was computed as the weighted sum of seven ES indicators and classified into five importance grades: Minor importance, Some importance, Moderate importance, High importance, and Critical importance (Fig. 10). From 2000 to 2020, the CES mean decreased from 0.6743 to 0.6613. The share of Critical-importance areas declined from 15.59% to 13.60%, while High-importance areas increased from 36.03% to 40.03%. The share of Minor-importance areas contracted sharply during 2000-2010 and then stabilized, consistent with early policy control effects. Across the 2030 simulations, the overall downward tendency in CES continues, with clear differences among scenarios. EP records the highest CES mean at 0.6599 and the smallest decline in Critical-importance areas. CP follows with a CES mean of 0.6597 and a Critical-importance share of 13.41%. Under UD, the share of Minor-importance areas increases to 6.09%, further compressing Critical-importance areas. ND shows the lowest CES mean at 0.6594 and the largest reduction in Critical-importance areas, with a final share of 3.52%.

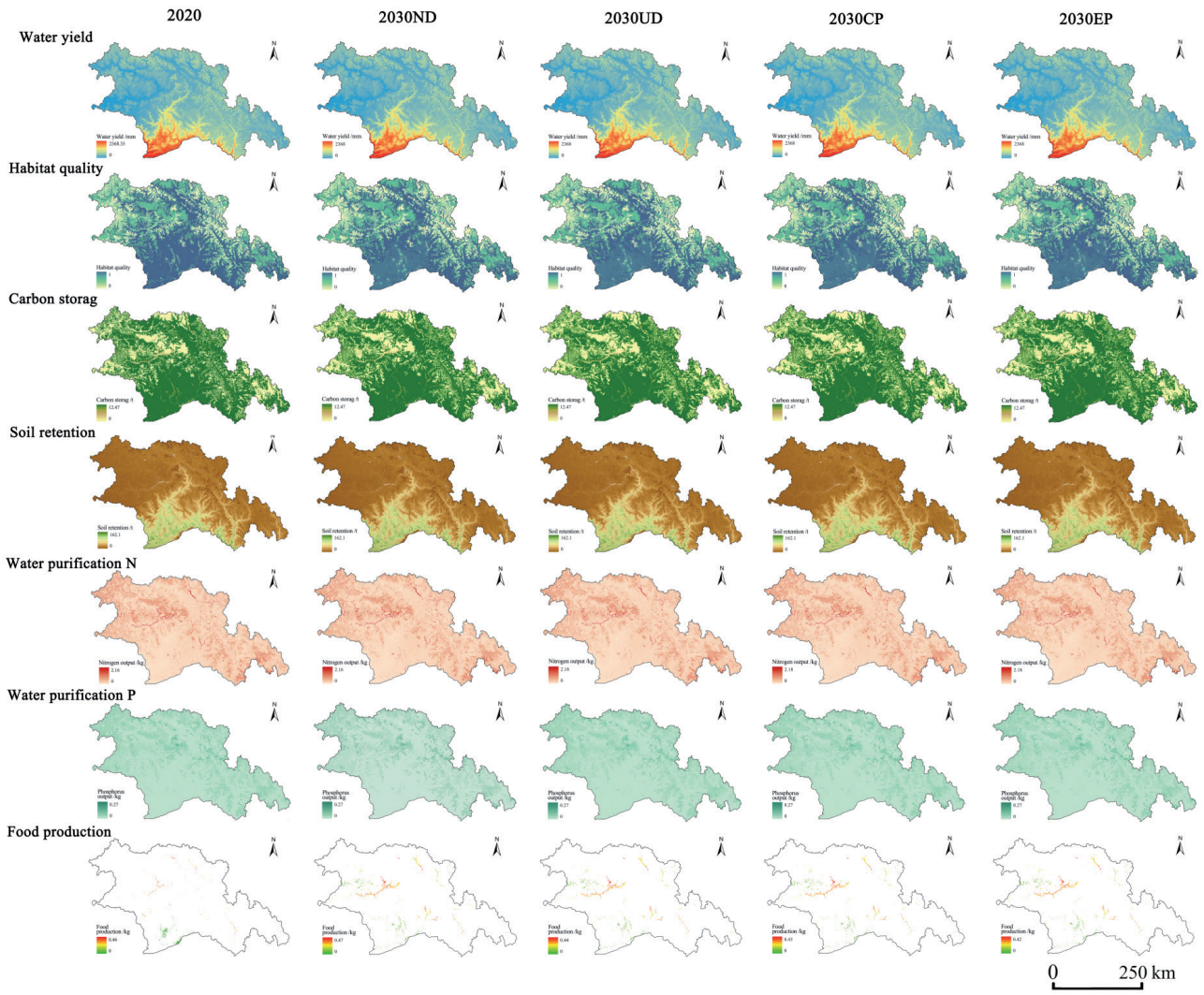

Fig. 9. Spatial distribution of ES changes under multiple scenarios in 2030.

CES Hotspot and Coldspot Spatial Pattern Analysis

Fig. 11 shows that CES hotspot areas in Nyingchi are simulated to contract toward southern lower-elevation regions by 2030, with previously contiguous hotspot tracts in Medog becoming increasingly fragmented. By contrast, coldspot areas expand toward northern higher-elevation zones and along urban-transportation corridors, with notable concentrations in the bare-rock belts of Nang County, the urban peripheries of Bayi District, western Mainling, and the eastern glacier forelands of Bome. Under the UD, coldspots cluster more strongly due to built-up land expansion, with the 99%-confidence and 95%-confidence coldspot areas increasing by 5.90% and 2.62%, respectively, while the overall extent of identified hotspots and coldspots contracts by 3.45%. Under the CP, 95%-confidence hotspot areas decline by 11.66%, and total hotspot area decreases by 1.04%. Under the EP, the distributions of hotspots and coldspots are more balanced, with 99%-confidence coldspot and hotspot areas reduced by 5.78% and 2.21%, respectively. Further spatial differentiation highlights the southeastern counties of Medog and Zayu as ecological value highlands, in contrast to the central-western counties of Bayi and Mainling, which are economic highlands. The ranking of coldspot area among scenarios is UD>ND>CP>EP, whereas that of hotspot area is EP>CP>UD>ND. This spatial gradient can inform differentiated ecological management strategies.

EOF Spatiotemporal Evolution Analysis of CES

Eigenvalue structure and mode separability. Across all four scenarios, EOF_1 explains ~80% of the variance and EOF_2 ~14% (each remaining mode <5%); adjacent error bands do not overlap, indicating statistically distinct leading modes. Mode interpretation. EOF_1 shows broadly consistent spatial loadings aligned with region-wide CES co-variation (Fig. 12(a-h)). Its temporal coefficient (PC_1) rises from about -1.5 to 0.5 over 2000-2010 and then stabilizes through 2030. EOF_2 exhibits loading patterns similar to EOF_1 but evolves out of phase with PC_1 during 2000-2010; after 2010,

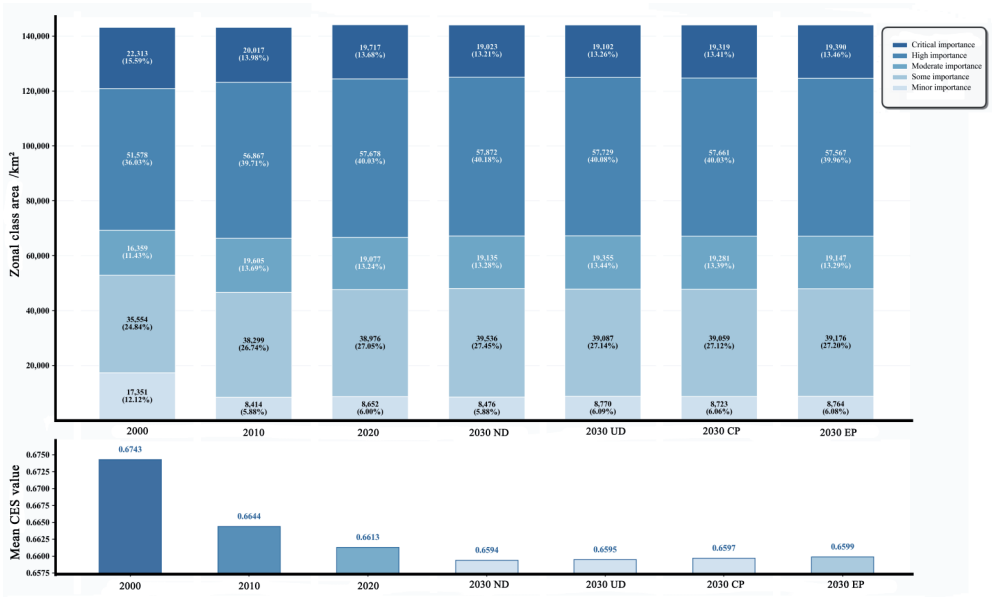

Fig. 10. CES classification and mean values under multiple scenarios for the base year and 2030.

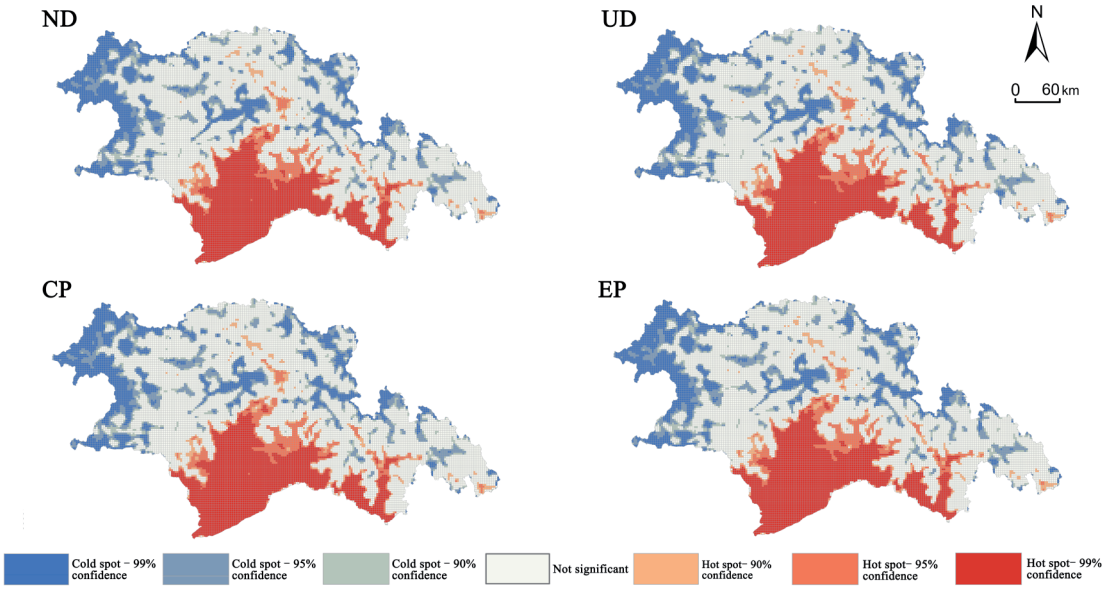

Fig. 11. Hotspot and coldspot distribution of CES under multiple scenarios in 2030.

PC_2 switches from negative to positive while decreasing in magnitude, gradually realigning with EOF_1. This transient phase reversal coincides with rapid urban expansion in 2000-2010, and the signal weakens after 2010 as ecological restoration accelerates and urban growth slows. EOF_3 explains only a small fraction of variance and is predominantly noise; subsequent analyses therefore focus on EOF_1.

Scenario-based spatial differences are evident. Under the EP, the largest share of positive-loading areas, 19.25%, occurs primarily in high-vegetation zones in southwestern Bome, southern Mainling, and southeastern Zayu. Under the UD and ND, negative-loading areas account for 13.00% and 12.87%, respectively, concentrated along urban expansion fronts in Bayi District, in valley floors of Mainling, and in higher-elevation, sparsely populated zones in Gongbo'gyamda and Nang County. Under the CP, low-variability areas form the largest share, 68.42%, concentrated mainly in southern Medog and Zayu. Overlaying EOF_1 loading distributions with CES hotspot and coldspot maps shows that strongly negative-loading areas align with coldspots, suggesting persistently lower ES levels in these regions. By contrast, hotspot regions such as Medog and Zayu, despite high baseline CES values, lie within mildly negative-loading zones,

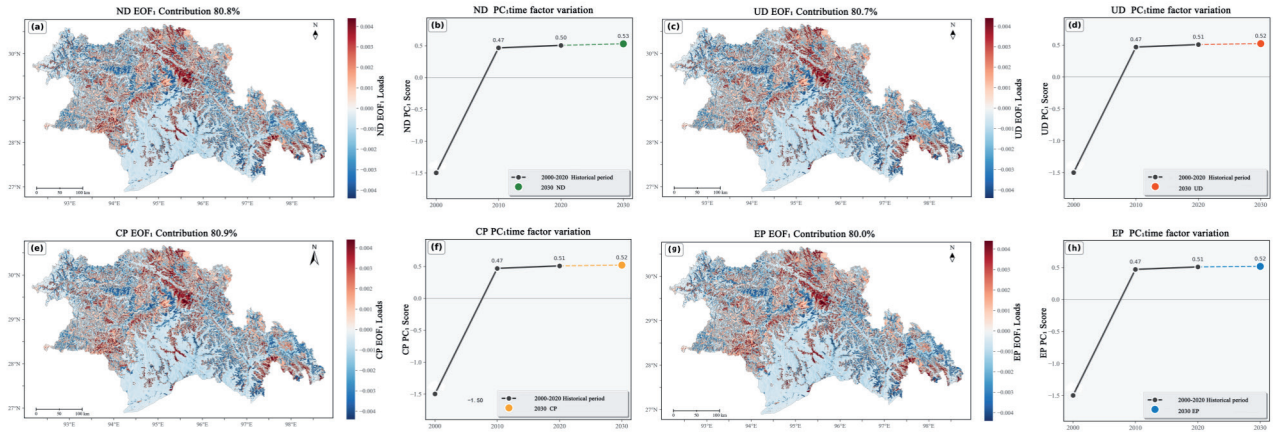

Fig. 12. EOF_1 spatial modes under multiple scenario projections for 2030.

indicating a tendency toward high-value decline even as PC_1 increases. Taken together, these spatial patterns are consistent with anthropogenic pressures – particularly urban expansion – shaping CES spatial heterogeneity.

To quantify county-level differences, the mean and dispersion of EOF_1 loadings – summarizing overall sensitivity direction and internal heterogeneity – were calculated and used for a binary-coupling analysis (Fig. 13). Because PC_1 is positive during the scenario period, EOF_1 loadings were classified into three zones using the natural-breaks method: enhancement, stabilization, and degradation (Fig. 14). Under the ND and CP, most counties show positive loading means with medium to low dispersion, indicating overall enhancement with limited within-county heterogeneity. In Bome County and Mainling County, enhancement areas account for 33.54% and 33.26%, respectively, patterns consistent with relatively strong ecological baselines and signs of self-recovery. By contrast, Zayu County shows a negative loading mean and the highest dispersion, suggesting a tendency toward ecological decline and spatial fragmentation under natural-succession dynamics, which may coincide with higher susceptibility to geohazards. Under the UD, county-level loading means generally decrease while dispersion increases markedly, accompanied by substantial expansion of degraded areas, a pattern consistent with negative urbanization pressures on ESs. In Bayi District, degraded areas expand by 1,640.52 km², and dispersion is the highest, highlighting pronounced spatial heterogeneity associated with an urban mosaic pattern. Under the EP, loading means increase across all counties and dispersion converges, indicating coordinated enhancement with spatial homogenization. Bome County reaches a loading mean of 0.579, and its enhancement areas expand to 34.3%, while the ecologically vulnerable Zayu County also shows a positive response, suggesting potential effects of active ecological interventions.

At the county scale, the leading EOF modes of CES evolution correspond to distinct development trajectories. In Bayi District, persistent CES coldspots and negative EOF_1 loadings coincide with rapid expansion of built-up land and the fragmentation of cropland and forest along major transport corridors and around the urban core. Although ecological protection policies have been introduced across Nyingchi, the concentration of population, infrastructure, and services in the municipal center makes it difficult for previously degraded areas to recover, resulting in a form of "degradation path dependence": once high-value ecosystems are fragmented and converted to dense built-up land, the rigidity of long-lived infrastructure, sunk investment costs and the inherent time lag in ecological recovery tend to lock the landscape into a low-CES state, so that coldspots persist in the EOF patterns. By contrast, in Mainling and Bome, relatively stable or improving CES values are associated with slower urban expansion and more continuous forest-grass mosaics, while Zayu exhibits a mixed pattern in which localized high-intensity disturbance coexists with partial recovery. These contrasts suggest that the spatial modes extracted by EOF reflect different stages along a path-dependent degradation-stabilisation continuum among counties.

Based on a bivariate matrix of mean loading and loading dispersion, the seven administrative divisions were classified into three management-unit types, each with differentiated strategies: (i) synergistic-heterogeneous – high mean and high dispersion – Mainling and Bome County. Priorities include strict protection of high-value patches, establishment of a dynamic monitoring system, and exploration of pathways for ecological-asset development; (ii) inverse-heterogeneous – low mean and high dispersion – Bayi District and Zayu. Priorities include tighter urban growth boundary control and expansion of the green-infrastructure network in Bayi, together with targeted ecological restoration and stricter regulation of high-intensity disturbances in Zayu; and (iii) inverse-steady-state – low mean and low dispersion – Medog, Nang County, and Gongbo'gyamda. Minimal-intervention

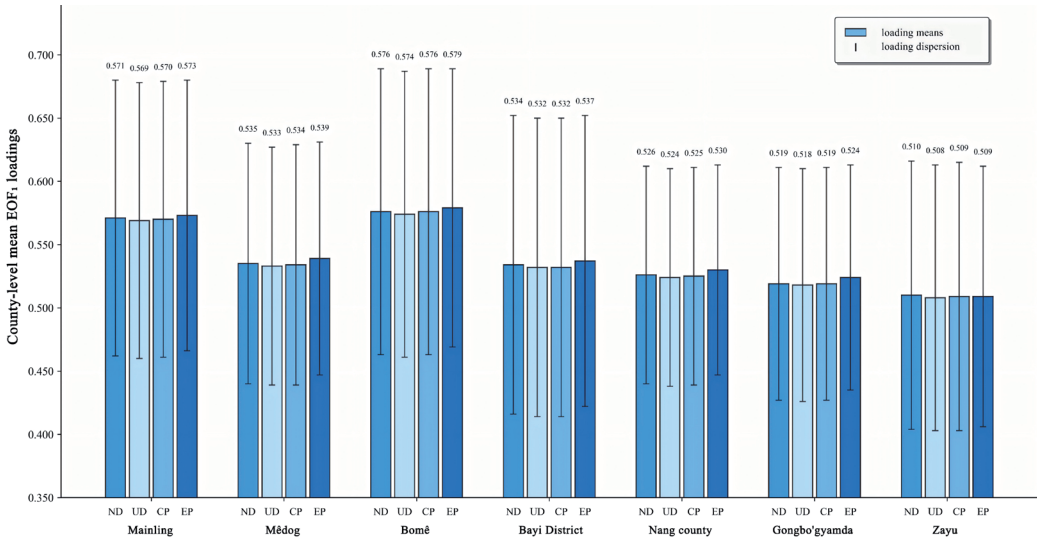

Fig. 13. Mean and standard deviation of EOF1 by county under multiple scenarios in 2030.

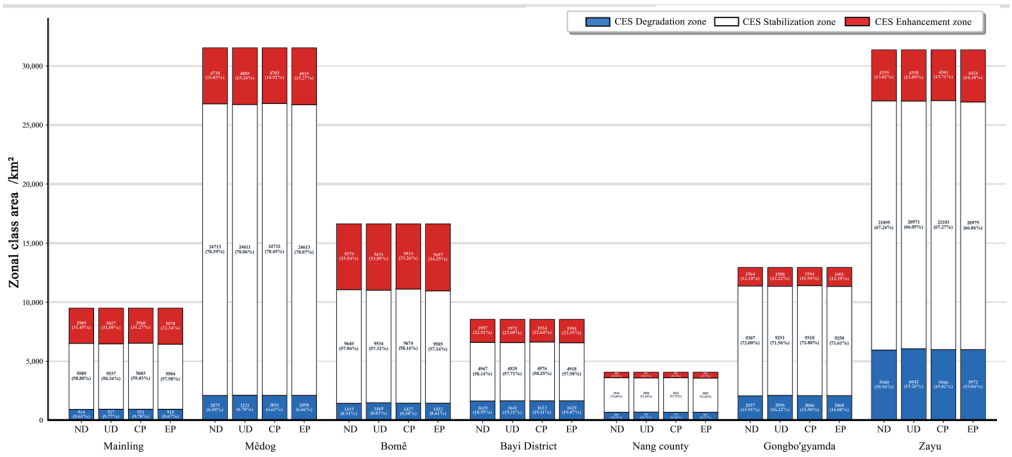

Fig. 14. EOF1 classification by county under multiple scenarios in 2030.

strategies are recommended, including maintaining natural succession, conducting regular ecological-health assessments, setting early-warning thresholds, and strictly limiting large-scale development.

Discussion

Land Use Change Impacts on ESs

EOF_1 shows that PC_1 shifted from negative to positive values during 2000-2010, coinciding with a net expansion of built-up land of 18.68 km² over the same interval. This temporal correspondence suggests that land-use transformation was a major driver of ES dynamics during this period. Spatially, built-up expansion concentrated along river valleys and low-elevation belts, accompanied by conversions from forestland, grassland, and cropland to built-up land. Over the same period, regulating services such as water yield and soil retention declined along the elevational gradient. EOF_1 explains a substantial share of the variance, and clusters of negative spatial loadings overlap with CES coldspots.

In terms of underlying processes, topography likely mediates this leading mode by shaping both development accessibility and background ecosystem processes: river valleys and low-elevation belts tend to concentrate anthropogenic disturbance, whereas higher-elevation areas are more constrained by terrain and dominated by natural dynamics. Within this topographic setting, NDVI provides an ecological bridge linking land-use transitions to CES responses, as vegetation condition is closely coupled to multiple regulating and supporting functions. Corridor-focused built-up expansion and the associated landscape fragmentation may reduce vegetation continuity and weaken regulating processes, which could reinforce persistently low CES patterns in vulnerable zones. In addition, intensifying urbanization may increase nitrogen and phosphorus

loads, contributing to the continued weakening of water-purification services. At the landscape scale, reduced connectivity across ecologically sensitive zones may further constrain service flows. Taken together, these mechanisms are consistent with a topography-mediated degradation pathway in which topographic gradients shape the spatial distribution of land-use intensity and, in turn, influence CES patterns.

CES Response Mechanisms and Sustainable Management Strategies

The evolution of CES displays pronounced vertical zonation. Lower-elevation valleys are shaped mainly by anthropogenic disturbance, whereas higher-elevation regions are influenced more by natural ecological processes. In plateau systems with relatively low resistance and low resilience, compounded by complex geomorphology, tectonically active counties such as Zayu tend to show low mean EOF_1 loadings and a high proportion of degraded areas, consistent with the greater frequency of geological hazards. By contrast, Medog is identified as a CES hotspot yet appears in the negative-loading zone in the EOF_1 results, and PC_1 remains at a persistently high level. Together, these features suggest potential vulnerability and a risk of decline despite a high baseline. This interpretation is consistent with Duan et al. [63], who reported that the Yarlung Zangbo Grand Canyon – centered on Medog – delivers substantial ESs but experiences frequent geohazards and elevated ecological risk. Hence, hotspot status does not necessarily imply ecological security: high-value areas may be more susceptible to degradation where the natural setting is fragile or external pressures are strong. Areas with strongly negative EOF_1 loadings tend to overlap with identified CES coldspots, suggesting degradation-path dependence in low-service regions. Initial declines can trigger positive feedbacks that reinforce degradation and create traps that are difficult to reverse. This pattern is most evident in Bayi District's built-up core, where ecosystem-service levels continue to fall, and recovery is challenging. Similar co-degradation dynamics have been documented by Zhu et al. [64] for alpine grasslands on the Tibetan Plateau: once productivity losses cross critical thresholds, feedbacks can rapidly push systems toward a low-service, hard-to-recover lock-in state. These observations indicate that low-CES regions entering a degradation trajectory are unlikely to recover through natural processes alone and therefore suggest the need for heightened attention; such areas may be considered for priority intervention, subject to site-specific assessment. To maintain rigor, we treat this as an interpretive hypothesis grounded in the observed spatial correspondence between EOF_1 loadings and CES coldspots. Formal quantitative substantiation will be pursued in follow-up work using segmented regression to probe potential thresholds and landscape metrics of fragmentation and connectivity to test for lock-in dynamics.

Beyond diagnosing these challenges, multi-scenario simulations provide deeper insight into the effectiveness of policy interventions. Under the EP, spatial patterns tend to homogenize, suggesting that protection measures may improve spatial balance and potentially strengthen overall ESs provision. By contrast, the UD is characterized by a polarization of CES outcomes, with urban expansion associated with regional declines. Notably, even with ecological protection, CES continues to trend downward, underscoring the intrinsic vulnerability of plateau ecosystems to land use change. Building on the EOF-derived mean–dispersion classification, tailored strategies are advisable to address local variation. Where both the mean and the dispersion are high, priorities may include strict protection of high-value patches, a dynamic monitoring system, and adaptive resource use. Where the mean is low, but dispersion is high, priorities may include robust urban growth boundaries, expansion of the green-infrastructure network, targeted ecological restoration, and tighter control of high-intensity disturbances. Where both the mean and the dispersion are low, minimal-intervention approaches that allow natural recovery are preferable. This management framework is intended to align with Nyingchi's Territorial Spatial Planning for 2021-2035. Implementation could prioritize ecological-redline control, establish multi-tier ecological-compensation mechanisms, and promote ecological industrialization. An integrated governance model – combining government leadership, market regulation, and broad social participation – can help coordinate spatial control, economic incentives, and community mobilization, creating reinforcing links between planning, finance, and on-the-ground action. Taken together, these measures may help strengthen ecosystem resilience while supporting more balanced socio-economic development on the plateau.

The EOF-derived management typology provides an evidence-informed bridge from spatial diagnostics to policy options for highland cities. The differentiated strategies outlined here could support progress toward Sustainable Development Goal (SDG) 15 (Life on Land) by informing ecosystem restoration, land-degradation neutrality, and biodiversity conservation in highland regions. In parallel, the emphasis on spatial zoning, urban containment, and integrated management is consistent with SDG 11 (Sustainable Cities and Communities) and may contribute to resilience and sustainability in rapidly urbanizing highland settings. Taken together, the analytical framework and associated policy suggestions may offer a transferable – though context-dependent – pathway that helps advance sustainable land governance and promotes more resilient regional development in highland cities.

Transferability and Global Relevance

The analytical framework developed in this study appears applicable beyond the Qinghai-Tibet Plateau

and may be extended to other high-mountain socio-ecological systems. Evidence from the European Alps suggests that interactions between topographic gradients and rapid land use change are associated with pronounced vertical zonation of ESs, with functional degradation thresholds observed under intensified human pressures (Anselmetto et al., 2024) [65]. In the Andes, the expansion of high-altitude grazing, coupled with greater climatic variability, has been linked to abrupt declines in grassland productivity and to multiple services approaching critical tipping points (Duchicela et al., 2024) [66]. Similarly, in the Rocky Mountains' alpine and subalpine belts, land development together with climate warming is associated with increased ecosystem vulnerability and a greater likelihood of regime shifts (Oldfather et al., 2025) [67]. By integrating spatially explicit land use change simulation, early-warning indicators for ESs, and scenario-based management evaluation, the approach presented here offers a modular, transferable workflow. It can be adapted to support rapid diagnosis, risk screening, and the prioritization of adaptive strategies across diverse mountain regions. Placing the findings from Nyingchi in a broader global context, this framework provides both conceptual insight and practical guidance, helping to strengthen regional adaptation to environmental change and disaster risk under accelerating climate and land use pressures.

Innovations and Shortcomings

The PLUS-InVEST-EOF coupled framework developed in this study offers an integrated toolkit for a "pattern-process-mechanism" analytic paradigm. By applying EOF decomposition to extract dominant spatiotemporal modes and tracking their evolution using principal components (PCs), the approach moves beyond the constraints of purely static assessments and enables a dynamic evaluation of ESs. This strengthens comprehensive spatiotemporal analysis of CES and provides a transferable workflow for regional ecosystem-service assessment. In addition, we specified multi-dimensional development scenarios grounded in local conditions to generate more realistic projections of ecosystem-service trajectories. The aim is to inform land use management and sustainable ecosystem development in Nyingchi.

However, this study has several limitations that warrant refinement in future research: 1) Drivers of land use change in high-elevation systems are complex and uncertain. Future work could incorporate a broader set of drivers to improve predictive performance. 2) Some InVEST and PLUS parameters were set using regional literature and expert judgment, which may introduce subjectivity. Subsequent studies could employ sensitivity analysis and local calibration to refine parameterization and enhance robustness. 3) The analysis is constrained by four CES time slices, and data sparsity may limit the identification of higher-order modes. Increasing temporal sampling density would help improve the robustness and multi-scale interpretability of EOF results. 4) This study has not yet conducted a systematic quantification of uncertainty for the 2030 scenario projections, the CES composite index, or the hotspot identification results (e.g., via parameter perturbation, ensemble simulations, or interval estimation). Subsequent work will prioritize this component, which is important for enhancing the robustness and generalizability of the findings.

Conclusions

(1) Urbanization has become a primary driver reshaping land use in Nyingchi. From 2000 to 2010, the dynamic degree of built-up land reached 28.23% and then declined to 11.55% during 2010-2020, yet the built-up area still expanded by 28.96 km². By 2030, built-up land is projected to increase by an additional 30.49 km² under the UD scenario relative to 2020, whereas the EP scenario substantially constrains this expansion, highlighting the critical role of policy intervention in regulating land conversion.

(2) From 2000 to 2020, regulating services declined markedly, with water yield decreasing by 29.7% and soil retention by 49%. By contrast, supporting services showed divergent trajectories: habitat quality remained high (0.734 in 2010), while carbon storage varied within a narrow range (11.036-11.207 t). Across the 2030 scenarios, UD consistently produces less favorable service outcomes, whereas EP yields the highest overall service levels. Taken together, these findings underscore that sustaining ESs in fragile high-altitude systems will depend on keeping development intensity within ecological limits and strengthening conservation-oriented constraints.

(3) The CES index declined during 2000-2020, accompanied by a contraction of critically important areas. For 2030, relative to 2020, EP yields the highest average CES (0.6599) and the smallest reduction in critically important area, whereas UD shows the opposite pattern; CP remains intermediate and near a quasi-steady state. Overall, the scenario contrast indicates that conservation-oriented policies can slow CES deterioration, but reversing the long-term decline will likely require additional, more targeted measures.

(4) During 2000-2020, CES hotspots contracted and became increasingly fragmented, concentrating in low-elevation southern areas, whereas coldspots expanded across the high-elevation northwest and along the Bayi–Mainling corridor – consistent with a "southward retreat, northward advance" reconfiguration. Across scenarios, EP tends to curb coldspot expansion, whereas UD amplifies it. Overall, the hotspot and coldspot mosaic appears to be jointly shaped by elevation gradients and corridor-driven urban spillover, highlighting the planning importance of managing valley-corridor expansion pressures in high-altitude vulnerable zones.

(5) EOF_1 explains over 80% of the total variance, and PC_1 increased sharply during 2000-2010 in parallel with rapid built-up expansion, suggesting that land-use change was a dominant correlate of the leading ES mode in this period. Spatially, high-magnitude EOF_1 loading zones overlap with CES coldspots, which we interpret as being consistent with a potential path-dependent degradation trend in low-CES regions. Notably, CES hotspots such as Medog County also show declines from initially high CES baselines, indicating latent vulnerability even in high-value ecosystems. Building on these spatial signals, we combined county-level mean EOF_1 loadings with their dispersion to delineate three management units, providing a pragmatic basis for more targeted zoning-oriented ecological governance.

Acknowledgments

This study was funded by the Ministry of Education Humanities and Social Sciences Research Planning Fund, Xizang Project (23XZJA840001); the Key Laboratory of Ecology and Energy Conservation in High-Density Human Settlements, Ministry of Education (20210111); and the 2025 Special Fund for Local University Development and Reform, Central Government of China: Plateau-Characteristic Agro-Pastoral Science and Technology Institute Construction and Service Capacity Enhancement (YJSX K2025-12).

Data Availability

The data that support the findings of this study are available from the Resource and Environment Science Data Platform (RESDC), the National Earth System Science Data Center (Geodata), the National Cryosphere Desert Data Center (NCDC), JAXA EORC (AW3D30), and the China Standard Map Service. Access to these datasets is governed by the providers' terms (e.g., registration, license, and/or fees). These datasets were used under license for the present study, and the authors are not permitted to redistribute them. Access requests should be made directly to the respective providers via the services listed above. Model configuration files, parameter settings, and analysis scripts that do not contain third-party raw data are available from the corresponding author upon reasonable request.

Conflict of Interest

The authors declare no conflict of interest.

References

1. FISHER J.C., DALLIMER M., IRVINE K.N., AIZLEWOOD S.G., AUSTEN G.E., FISH R.D., KING P.M., DAVIES Z.G. Human well-being responses to species' traits. Nature Sustainability, **6** (10), 1219, **2023**.
2. LI J., WANG J., ZHOU W. Different impacts of urbanization on ecosystem services supply and demand across old, new and non-urban areas in the ChangZhuTan urban agglomeration, China. Landscape Ecology, **39** (6), 107, **2024**.
3. LV L., GUO W., ZHAO X., LI J., JI X., CHAO M. Integrated assessment and prediction of ecological security in typical ecologically fragile areas. Environmental Monitoring and Assessment, **196** (3), 286, **2024**.
4. ZHOU J.W., LUO J., MA X.Y. Spatiotemporal evolution and driving factors of land use and ecosystem service value in the Lhasa River Basin. Arid Zone Research, **41** (6), 1021, **2024**.
5. CHEN Y., QIAO X., YANG Y., ZHENG J., DAI Y., ZHANG J. Identifying the spatial relationships and drivers of ecosystem service supply-demand matching: A case of Yiluo River Basin. Ecological Indicators, **163,** 112122, **2024**.
6. SU W., QIU C.X., ZHAO L. Land use change and multi-scenario prediction in the "one river and two tributaries" basins of Tibet 2000-2020. Bulletin of Surveying and Mapping, **2024** (6), 90, **2024**.
7. GUAN R.J., CHEN Y.L., HUANG X.B., LIAN W.H., LIU X.G. Multi-scenario simulation of land use and ecosystem services response in southern Jiangxi based on the PLUS-InVEST model. Environmental Science, **46** (11), 7270, **2025.**
8. SHAFIZADEH-MOGHADAM H., ASGHARI A., TAYYEBI A., TALEAI M. Coupling machine learning, tree-based and statistical models with cellular automata to simulate urban growth. Computers, Environment and Urban Systems, **64**, 297, **2017**.
9. ASIF M., KAZMI J.H., TARIQ A., ZHAO N., GULUZADE R., SOUFAN W., ALMUTAIRI K.F., SABAGH A.E., ASLAM M. Modelling of land use and land cover changes and prediction using CA-Markov and Random Forest. Geocarto International, **38** (1), 2210532, **2023**.
10. LIANG X., TIAN H., LI X., HUANG J.-L., CLARKE K.C., YAO Y., GUAN Q., HU G. Modeling the dynamics and walking accessibility of urban open spaces under various policy scenarios. Landscape and Urban Planning, **207**, 103993, **2021**.
11. SU S., SUN Y., LEI C., WENG M., CAI Z. Reorienting paradoxical land use policies towards coherence: A self-adaptive ensemble learning geo-simulation of tea expansion under different scenarios in subtropical China. Land Use Policy, **67**, 415, **2017**.
12. JIN Q., LIU G., LI L., HE C., HUANG Y., YAO Y. Land use scenarios simulation based on the CLUE-S model of the Lijiang River Basin in Guilin, China. IOP Conference Series: Earth and Environmental Science, **46** (1), 012051, **2016**.
13. HWANG J., CHOI Y., KIM Y., LIM N.O., YOO Y.-J., CHO H.J., SUN Z., JEON S. Analysis of the effect of environmental protected areas on land use and carbon storage in a megalopolis. Ecological Indicators, **133**, 108352, **2021**.
14. YAN X., LI M., GUO D., YANG D., ZHAN D. Spatial-temporal evolution and prediction of carbon storage in Mohe city by linking the logistic-CA-Markov and InVEST models. Frontiers in Earth Science, **12**, 1383237, **2024**.
15. YANG X., CHEN R., ZHENG X.Q. Simulating land use change by integrating ANN-CA model and landscape

pattern indices. Geomatics, Natural Hazards and Risk, **7** (3), 918, **2016**.
16. JIANG X.T., ZHAI S.Y., WANG Z., LIU H., CHEN J., ZHU Y.Y. Simulating the production-living-ecological space and analyzing eco-environmental effects based on the FLUS model in Zhengzhou, China. Acta Ecologica Sinica, **43** (15), 6225, **2023**.
17. AI X., ZHENG X., ZHANG Y., LIU Y., OU X., XIA C., LIU L. Climate and land use changes impact the trajectories of ecosystem service bundles in an urban agglomeration: Intricate interaction trends and driver identification under SSP-RCP scenarios. Science of The Total Environment, **944**, 173828, **2024**.
18. LIN J., LI X., WEN Y., HE P. Modeling urban land use changes using a landscape-driven patch-based cellular automaton (LP-CA). Cities, **132**, 103906, **2023**.
19. XU W., XU H., LI X., QIU H., WANG Z. Ecosystem services response to future land use/cover change (LUCC) under multiple scenarios: A case study of the Beijing–Tianjin–Hebei (BTH) region, China. Technological Forecasting and Social Change, **205**, 123525, **2024**.
20. JIN A., ZHANG G., MA P., WANG X. Ecosystem services trade-offs in the Chaohu Lake Basin based on land-use scenario simulations. Land, **13** (12), 2210, **2024**.
21. YANG Y., WANG H., LI X., HUANG X., LYU X., TIAN H., QU T. How will ecosystem carbon sequestration contribute to the reduction of regional carbon emissions in the future? Analysis based on the MOP-PLUS model framework. Ecological Indicators, **156**, 111156, **2023.**
22. JIN A., WANG P., ZHANG G., SHI H., LI H. Ecological quality and spatial structure dynamics under future scenarios: A topological perspective from the Yellow River Basin. Journal of Cleaner Production, **522**, 146346, **2025**.
23. SHERROUSE B.C., SEMMENS D.J., CLEMENT J.M. An application of Social Values for Ecosystem Services (SolVES) to three national forests in Colorado and Wyoming. Ecological Indicators, **36**, 68, **2014**.
24. AZNAREZ C., KUMAR S., MARQUEZ-TORRES A., PASCUAL U., BARÓ F. Ecosystem service mismatches evidence inequalities in urban heat vulnerability. Science of The Total Environment, **922**, 171215, **2024**.
25. HAMEL P., GUERRY A.D., POLASKY S., HAN B., DOUGLASS J.A., HAMANN M., JANKE B., KUIPER J.J., LEVREL H., LIU H., LONSDORF E.V., MCDONALD R.I., NOOTENBOOM C., OUYANG Z., REMME R.P., SHARP R.P., TARDIEU L., VIGUIÉ V., XU D., ZHENG H., DAILY G.C. Mapping the benefits of nature in cities with the InVEST software. npj Urban Sustainability, **1**, 25, **2021**.
26. ZANK B., BAGSTAD K.J., VOIGT B., VILLA F. Modeling the effects of urban expansion on natural capital stocks and ecosystem service flows: A case study in the Puget Sound, Washington, USA. Landscape and Urban Planning, **149**, 31, **2016**.
27. AN J.J., YANG Y., YUAN X.F., SU Q.J., AN Q.M. Spatiotemporal evolution, agglomeration characteristics, and trade-offs and synergies of ecosystem services in Northern Shaanxi. Research of Soil and Water Conservation, **32** (1), 316, **2025.**
28. WILLCOCK S., HOOFTMAN D.A.P., NEUGARTEN R.A., CHAPLIN-KRAMER R., BARREDO J.I., HICKLER T., KINDERMANN G., LEWIS A.R., LINDESKOG M., MARTÍNEZ-LÓPEZ J., BULLOCK J.M. Model ensembles of ecosystem services fill global certainty and capacity gaps. Science Advances, **9** (14), eadf5492, **2023**.
29. LI J., HU J., KANG J., SHU W. Spatio-temporal variation and prediction of land use and carbon storage based on PLUS–InVEST model in Shanxi Province, China. Landscape Ecology and Engineering, **21** (1), 107, **2025**.
30. LIU J., SUN J., LIU G., JIANG T. Assessment of carbon stock of ecological system of Jinan based on InVEST model. Environmental Science Survey, **42**, 17, **2023**.
31. GRÊT-REGAMEY A., SIRÉN E., BRUNNER S.H., WEIBEL B. Review of decision support tools to operationalize the ecosystem services concept. Ecosystem Services, **26**, 306, **2017**.
32. ZHANG Q., HUANG R., ZHU C., HUANG L., YANG D. Integrating land use simulation and carbon assessment for sustainable urban planning in Fuzhou metropolitan area using PLUS and InVEST models. Scientific Reports, **15** (1), 30382, **2025**.
33. MARTÍNEZ-LÓPEZ J., BAGSTAD K.J., BALBI S., MAGRACH A., VOIGT B., ATHANASIADIS I., PASCUAL M., WILLCOCK S., VILLA F. Towards globally customizable ecosystem service models. Science of the Total Environment, **650** (2), 2325, **2019**.
34. SÁNCHEZ-CANALES M., LÓPEZ BENITO A., PASSUELLO A., TERRADO M., ZIV G., ACUÑA V., SCHUHMACHER M., ELORZA F.J. Sensitivity analysis of ecosystem service valuation in a Mediterranean watershed. Science of the Total Environment, **440**, 140, **2012**.
35. LU C., SIDAI G., YANGLI L. Discerning changes and drivers of water yield ecosystem service: A case study of Chongqing–Chengdu District, Southwest China. Ecological Indicators, **160**, 111767, **2024**.
36. WANG X., LIU B., CHEN J., ARASH M., ZHANG B., CHANG Q., LIU J., YOU W. Assessing the impact of land use change on habitat quality in Zhongwei through multi-scenario simulation using the PLUS and InVEST models. Scientific Reports, **15** (1), 12355, **2025**.
37. YAO C.Y., HE Y.M., CHENG J.X., ZHANG T.Y., PAN H.Y., MA H.J. Evaluation and optimization of ecological security pattern in the Minjiang River Basin based on the minimum cumulative resistance and gravity models. Acta Ecologica Sinica, **43** (17), 7083, **2023**.
38. ADEM ESMAIL B., CORTINOVIS C., GENELETTI D., INOSTROZA L., PETERS R., ROMELLI C., SCHULZE I., TECLE-MISGHINA B., TEKLEMARIAM M., WANG J., ALBERT C. Mapping and analyzing ecosystem services hotspots and coldspots for sustainable spatial planning in the greater Asmara Area, Eritrea. Environmental Management, **75** (3), 551, **2025**.
39. WU H., AN H.X., SONG X.Y., WANG Z.Y., LI J.Y., CHENG D.L., MIAO X. Assessment of ecological protection importance and ecological function zoning in Nyingchi City. Science and Technology for Development, **18** (5), 686, **2022**.
40. SU L.B., GUO Y.G., WU Y., YANG Y.T. Analysis of geomorphological forms in the Nyang River Basin based on DEM. Science of Soil and Water Conservation, **18** (3), 12, **2020**.
41. HAO S.N., SU L.B., GUO Y.G. Impact of land use change on ecological sensitivity in the Niyang River Basin, Tibet. Bulletin of Soil and Water Conservation, **43** (2), 303, **2023**.
42. WU Q., SONG J., SUN H., HUANG P., JING K., XU W., WANG H., LIANG D. Spatiotemporal variations of water conservation function based on EOF analysis at multi time scales under different ecosystems of Heihe River Basin. Journal of Environmental Management, **325**, 116532, **2023**.

43. QIAO B., YAN Y.Q., ZHANG T.H., LI X.Y., ZHANG R., LI X., ZHOU B.R. Identification and optimization strategies for landscape ecological risk in Xining City based on land use change. Acta Ecologica Sinica, **42** (8), 2020, **2023**.
44. YANG S., SU H., ZHAO G.P. Multi-scenario simulation of urban ecosystem service value based on the PLUS model: A case of Hanzhong City. Journal of Arid Land Resources and Environment, **36** (10), 86, **2022**.
45. CAO X.F. Evaluation of ecological restoration effectiveness in Hefei's land spatial planning based on ecological security pattern and the PLUS model. Doctoral dissertation, Jilin University, **2023**.
46. SUN X.X., XUE J.H., DONG L.N. Spatiotemporal variation and prediction of ecosystem carbon storage in Nanjing City based on the PLUS and InVEST models. Journal of Ecology and Rural Environment, **39** (1), 41, **2023**.
47. OUYANG X., HE Q., ZHU X. Impact of land-use change on ecosystem service value under multiple scenarios: A case study of the Chang-Zhu-Tan urban agglomeration. Economic Geography, **40** (1), 93, **2020**.
48. CHOI C.Y., SHI X., SHI J., GAN X., WEN C., ZHANG J., JACKSON M.V., FULLER R.A., GIBSON L. China's Ecological Conservation Redline policy is a new opportunity to meet post-2020 protected area targets. Conservation Letters, **15** (2), e12853, **2022**.
49. LIU J., ZHOU J., HE Q. Impact of China's Permanent Basic Farmland Protection Redline and Ecological Protection Redline on Water Conservation in the Loess Gully Region. Land, **13** (9), 1424, **2024**.
50. BAI Y., WONG C.P., JIANG B., HUGHES A.C., WANG M., WANG Q. Developing China's ecological redline policy using ecosystem services assessments for land use planning. Nature Communications, **9**, 3034, **2018**.
51. WANG B., LIAO J., ZHU W. Setting neighborhood weights of the FLUS model based on historical scenarios: A case study of land-use simulation for the Min Delta urban agglomeration in 2030. Acta Ecologica Sinica, **39** (12), 4284, **2019**.
52. PEOPLE'S GOVERNMENT OF XIZANG AUTONOMOUS REGION. Approval of the "Nyingchi Territorial Spatial Master Plan (2021-2035)". People's Government of Xizang Autonomous Region, **2024**.
53. PEOPLE'S GOVERNMENT OF XIZANG AUTONOMOUS REGION. Approval of the Territorial Spatial Master Plans (2021-2035) for seven counties/districts/cities of Nyingchi. People's Government of Xizang Autonomous Region, **2024**.
54. HAN W.Y., XIA S.S., ZHOU W., SHEN Y., SU X.K., LIU G.H. Construction of the ecological security pattern of the Lhasa River Basin based on ecological corridor identification. Acta Ecologica Sinica, **43** (21), 8948, **2023**.
55. YANG Z. Evaluation of ecosystem service functions and influencing factors in Tibe. Beijing Forestry University, **2022**.
56. TANG H., HALIKE A., YAO K., WEI Q., YAO L., TUHETI B., LUO J., DUAN Y. Ecosystem service valuation and multi-scenario simulation in the Ebinur Lake Basin using a coupled GMOP-PLUS model. Scientific Reports, **14** (1), 5071, **2024**.
57. LIU J., LIU B., WU L., MIAO H., LIU J., JIANG K., DING H., GAO W., LIU T. Prediction of land use for the next 30 years using the PLUS model's multi-scenario simulation in Guizhou Province, China. Scientific Reports, **14** (1), 13143, **2024**.
58. ZHANG Y., LI J., PAN B. Evaluation of ecosystem services and multi-scenario prediction in the Yellow River Basin based on the PLUS model: A case study of the Shaanxi section. Arid Land Geography, **47** (11), 1935, **2024**.
59. LI Y., LIU W., FENG Q., ZHU M., YANG L., ZHANG J., YIN X. The role of land use change in affecting ecosystem services and the ecological security pattern of the Hexi Regions, Northwest China. Science of the Total Environment, **855**, 158940, **2023**.
60. YOU C., QU H., GUO L. A framework of composite factors for assessing ecosystem service supply drivers: A sustainable socio-ecological perspective. Ecological Indicators, **169**, 112811, **2024**.
61. JIA H., WANG T., LIANG P., ZHANG J., ZHANG R. Critical evaluation on the ecosystem service levels of provincial capital cities along the Yellow River Basin. Frontiers in Environmental Science, **13**, 1554157, **2025**.
62. CHANG J., WU Z., LI Q., LIANG H., DU Z., LEI T., SUN B. Spatiotemporal distribution and hotspot-coldspot analysis of ecosystem services in the Beijing-Tianjin wind-blown sand source region. Journal of Soil and Water Conservation, **38** (3), 216, **2024**.
63. DUAN S., HAN F., LI F., YANG Z. Spatial evaluation of the ecological value importance of the national park in Yarlung Tsangpo Grand Canyon. Journal of Environmental Management, **320**, 115943, **2022**.
64. ZHU Q., CHEN H., PENG C., LIU J., PIAO S., HE J.-S., WANG S., ZHAO X., ZHANG J., FANG X., JIN J., YANG Q.-E., REN L., WANG Y. An early warning signal for grassland degradation on the Qinghai–Tibetan Plateau. Nature Communications, **14**, 6406, **2023**.
65. ANSELMETTO N., WEISBERG P.J., GARBARINO M. Global change in the European Alps: A century of post-abandonment natural reforestation at the landscape scale. Landscape and Urban Planning, **243**, 104973, **2024**.
66. DUCHICELA S.A., LLAMBÍ L.D., BONNESOEUR V., ROMÁN-DAÑOBEYTIA F. Pastoralism in the high tropical Andes: A review of the effect of grazing intensity on plant diversity and ecosystem services. Applied Vegetation Science, **27** (3), e12791, **2024**.
67. OLDFATHER M.F., ENNIS A., MILLER B.W., CLARK-WOLF K., RANGWALA I., ROBE H., LITTLEFIELD C. Climate change impacts and adaptation in US Rocky Mountain high-elevation ecosystems. Arctic, Antarctic, and Alpine Research, **57** (1), 2450089, **2025**.

Supplementary Material

link to the material: https://www.pjoes.com/SuppFile/218207/1/